Cosmological simulations of galaxy clusters

Stefano Borgani[1,2,3] & Andrey Kravtsov[4,5,6]

1- Dipartimento di Astronomia dell'Università di Trieste, via Tiepolo 11, I-34131 Trieste, Italy
(borgani@oats.inaf.it)
2- INAF, Osservatorio Astronomico di Trieste, via Tiepolo 11, I-34131 Trieste, Italy
3- INFN – National Institute for Nuclear Physics, Trieste, Italy
4- Kavli Institute for Cosmological Physics, The University of Chicago, Chicago, IL 60637, USA
(andrey@oddjob.uchicago.edu)
5- Enrico Fermi Institute, The University of Chicago, Chicago, IL 60637, USA
6- Dept. of Astronomy & Astrophysics, The University of Chicago, 5640 S. Ellis Ave., Chicago, IL
60605, USA

Abstract

We review recent progress in the description of the formation and evolution of galaxy clusters in a cosmological context by using state-of-art numerical simulations. We focus our presentation on the comparison between simulated and observed X–ray properties, while we will also discuss numerical predictions on properties of the galaxy population in clusters, as observed in the optical band. Many of the salient observed properties of clusters, such as scaling relations between X–ray observables and total mass, radial profiles of entropy and density of the intracluster gas, and radial distribution of galaxies are reproduced quite well. In particular, the outer regions of cluster at radii beyond about 10 per cent of the virial radius are quite regular and exhibit scaling with mass remarkably close to that expected in the simplest case in which only the action of gravity determines the evolution of the intra-cluster gas. However, simulations generally fail at reproducing the observed "cool core" structure of clusters: simulated clusters generally exhibit a significant excess of gas cooling in their central regions, which causes both an overestimate of the star formation in the cluster centers and incorrect temperature and entropy profiles. The total baryon fraction in clusters is below the mean universal value, by an amount which depends on the cluster-centric distance and the physics included in the simulations, with interesting tensions between observed stellar and gas fractions in clusters and predictions of simulations. Besides their important implications for the cosmological application of clusters, these puzzles also point towards the important role played by additional physical processes, beyond those already included in the simulations. We review the role played by these processes, along with the difficulty for their implementation, and discuss the outlook for the future progress in numerical modeling of clusters.

keywords: astrophysics, cosmology, computer science, fluid dynamics

1 Introduction

1.1 Galaxy clusters in the hierarchy of cosmic structures

Astronomical observations over the last century have revealed the existence of a continuous hierarchy of cosmic structures involving a wide range of scales. On the scales of hundreds of

thousands of parsecs[1] the distribution of luminous matter is highly non-uniform and is concentrated in the "islands" which we call galaxies. Galaxies themselves are not distributed randomly but are concentrated in groups of two or more galaxies (roughly a million parsec in size), large concentrations of hundreds and sometimes thousands of galaxies (up to three–four million pc in size), which we call galaxy clusters, and a network of filaments (tens of millions of pc in size) interconnecting individual galaxies, groups, and clusters.

Clusters of galaxies occupy a special position in this hierarchy: they are the largest objects that have had time to undergo gravitational collapse. Existence of clusters of nebulae have been known for more than a hundred years. However, only after Edwin Hubble's proof that spiral and elliptical nebulae were bona fide galaxies like the Milky Way located at large distances from us (Hubble, 1925, 1926), it was realized that clusters of nebulae are systems of enormous size and mass. Back in the 1930s astronomers recognized that some invisible dark matter (DM) should dominate the overall gravitational field of clusters in order to explain unexpectedly high velocities of galaxies within the Virgo Cluster, thus making galaxy clusters "ante litteram" cosmological probes (Zwicky 1933; Smith 1936; Zwicky 1937; see Biviano 2000 for a historical overview). The interest in galaxy clusters has rapidly increased thereafter and large catalogs of clusters have been constructed using visual searches of deep photographic sky images for strong concentrations of galaxies (Abell, 1958; Zwicky et al., 1961). Clusters remain powerful cosmological probes and astrophysical laboratories today, as larger and more sensitive surveys of clusters are constructed.

1.2 Galaxy clusters as cosmological probes and astrophysical laboratories

Measurements of the velocities of galaxies in clusters have provided the first determination of the typical mass involved in such structures, which typically falls in the range[2] 10^{14}–$10^{15}M_\odot$. Stars and gas in galaxies, however, constitute only a small fraction (≈ 2 per cent) of this mass (Lin et al., 2003; Gonzalez et al., 2007). With the advent of X–ray astronomy in the late 60s, galaxy clusters have been also identified as powerful emitters of photons having energies of several kilo-electronvolts (keV; Gursky et al. 1971; Kellogg et al. 1971), with typical luminosities of about 10^{43}–$10^{45}\,\mathrm{erg\,s^{-1}}$. This emission was interpreted as due to the presence of a hot, fully-ionized thermal plasma with temperature of several keV ($1\ \mathrm{keV} \simeq 1.16 \times 10^{7}\mathrm{K}$) and a typical particle number density of 10^{-1}–$10^{-4}\mathrm{cm^{-3}}$, with the two main contributions to emission from the free-free interactions of electrons and ions and line emission by ions of heavy elements such as iron. This diffuse plasma is not associated with individual galaxies and constitutes the intra-cluster medium (ICM), which contains the bulk of the normal baryonic matter in clusters. The temperature of the ICM is consistent with velocities of galaxies and indicates that both galaxies and gas are in equilibrium within a common gravitational potential well. The mass of galaxies and hot gas is not sufficient to explain the implied depth of the potential well, which implies that most of the mass in clusters is in a form of dark matter. Given that hydrogen is by far the most abundant element in the universe, most of the plasma particles are electrons and protons, with a smaller number of helium nuclei. There are also trace amounts of heavier nuclei some of which are only partially ionized; the typical abundance of the heavier elements is about a third of that found in the Sun or a fraction of one per cent by mass.

Since its discovery, the X–ray emission serves as a highly efficient and clean way to identify galaxy clusters out to large cosmological distances (Rosati et al., 2002; Vikhlinin et al., 2008). In addition, the population of thermal electrons also leaves its imprint on the Cosmic Microwave Background (CMB), when observed in the direction of galaxy clusters: their inverse Compton

---

[1] A parsec (pc) is 3.086×10^{18} cm.

[2] $M_\odot \approx 1.99 \times 10^{33}$ g is the mass of the Sun.

scattering off the CMB photons induces small but measurable distortions in the black–body spectrum of the CMB, equivalent to temperature variations of about 10^{-4}–10^{-5} K, thus giving rise to the Sunyaev–Zeldovich effect (SZE; Sunyaev & Zeldovich, 1970, 1972, 1980, for a review see Carlstrom et al. 2002). Given that the SZE measurement is simply a measurement of the intensity or temperature fluctuation of the CMB, it is nearly distance independent, which makes it a powerful way to detect distant clusters. Indeed, a number of observational campaigns are now started or planned to search and study galaxy clusters using the SZE within a significant fraction of the cosmological past light-cone (Kosowsky, 2003; Ruhl et al., 2004; Staniszewski et al., 2008).

Figure 1 shows an overlay of the optical, X–ray and SZE images of the massive clusters Abell 1689 and 1914. It illustrates all of the main components of the clusters: the luminous stars, the hot ICM observed via its X-ray emission and the SZE, and even the presence of the unseen dark matter manifesting itself through gravitational lensing of background galaxies (see below). The figure shows several bright elliptical galaxies that are typically located near the cluster centers. A salient feature of such central galaxies is that they show little evidence of ongoing star formation, despite their extremely large masses. Furthermore, a large amount of DM, extending well beyond the region traced by the X–ray emission, leaves its imprint in the pattern of gravitational lensing, which causes the distortion of the images of background galaxies. In the inner regions of clusters the gravitational lensing is strong and its effects can be easily seen in the distorted images of background galaxies appearing as long thin arcs curved around the cluster center. At larger radii, the effect is weaker. Although not easily visible by eye, it can still be reliably measured by estimating shapes of many background galaxies and comparing their statistical average with the expected value for an isotropic distribution of shapes. The gravitational lensing is direct probe of the total mass distribution in clusters, which makes it both extremely powerful in its own right and a very useful check for other methods for measuring cluster masses.

Given their large mass, galaxy clusters represent the end result of the collapse of density fluctuations involving comoving scales of ~ 10 Megaparsecs (Mpc). For this reason, they mark the transition between two distinct dynamical regimes. On scales roughly above 10 Mpc, the evolution of the structure of the universe is mainly driven by gravity. In this regime, the evolution still feels the imprint of the cosmological initial conditions and can be described by analytical methods and, more accurately, by cosmological N-body simulations. The latter follow the growth of seed fluctuations in the matter density field from an early epoch to the present time (or even beyond) due to gravitational instabilities.

An example of how galaxy clusters trace cosmic evolution in cosmological simulations can be appreciated in Figure 2, which shows the evolution of the population of galaxy clusters, superimposed on the evolution of the matter density field for two different cosmological models. The upper panels are for a "concordance" spatially flat ΛCDM model, in which the mean mass density, in units of the critical density of the universe[3], is $\Omega_{\mathrm{m}} = 0.3$ and cosmological constant contributes the rest of the energy density required to make the universe flat, $\Omega_{\Lambda} = 0.7$. The lower panels also show a flat model, but without any cosmological constant (i.e., matter density is $\Omega_{\mathrm{m}} = 1$). Parameters of the two models have been chosen to produce a comparable number of clusters at the present time. Quite apparently, the number density of clusters evolves much more slowly in the ΛCDM model. Indeed, while this model predicts a significant population of clusters at redshift $z > 1$, and minimal evolution between $z = 0.6$ and $z = 0$, the abundance of such distant clusters rapidly and steadily drops in the $\Omega_m = 1$ Einstein-de Sitter model at $z > 0$. This is mainly because universe expands faster in models with lower mean matter density Ω_{m}. For

---

[3]The critical density, $\rho_c(z) = 3H(z)^2/8\pi G \approx 2.77 \times 10^{11}(h^{-1}M_\odot)/(h^{-1}\mathrm{Mpc})^3 \approx 1.88 \times 10^{-29}\, h^2\, \mathrm{g\, cm}^{-3}$, corresponds to the density for which the Universe is spatially flat and separates the models which will expand forever from those that will re-collapse at some point in the future. Here and in the following of this paper, h denotes the value of the Hubble constant at $z = 0$ in units of $100\ \mathrm{km\, s}^{-1}\mathrm{Mpc}^{-1}$
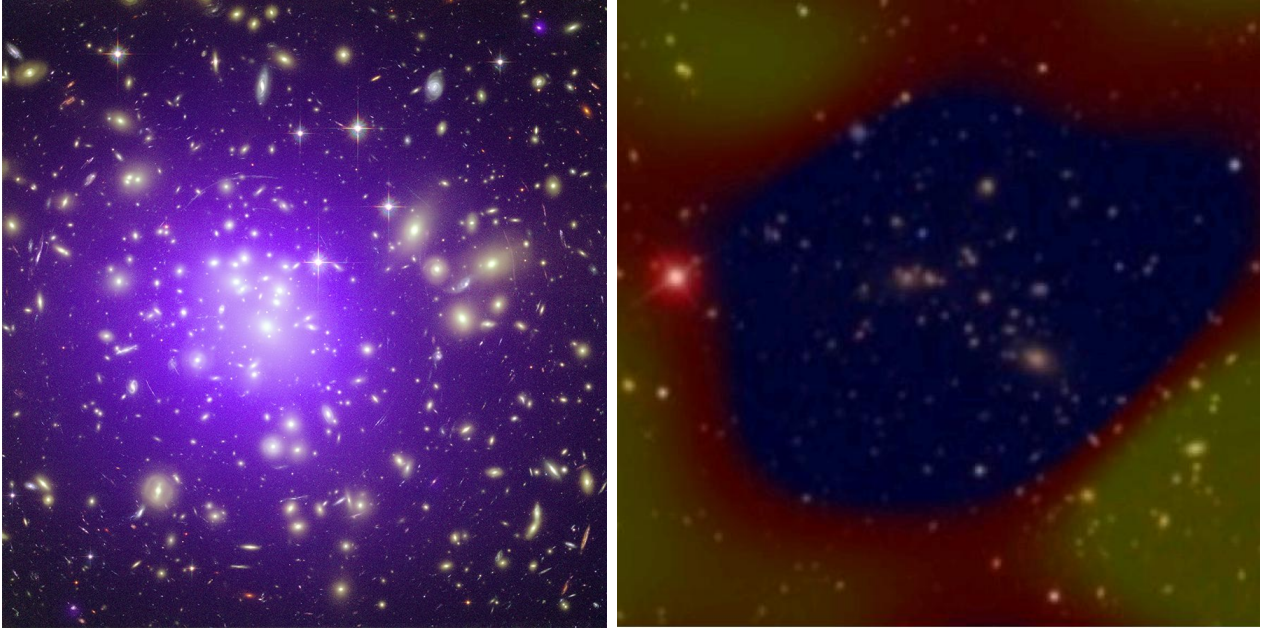
Figure 1: Left panel: composite X–ray/optical image of the galaxy cluster Abell 1689, located at redshift $z = 0.18$. The map shows an area of 556 kpc on a side. The purple diffuse halo shows the distribution of gas at a temperature of about 10^8 K, as revealed by the Chandra X-ray Observatory. Images of galaxies in the optical band, colored in yellow, are from observations performed with the Hubble Space Telescope. The long arcs in the optical image are caused by gravitational lensing of background galaxies by matter in the galaxy cluster, the largest system of such arcs ever found (Credit:X-ray: NASA/CXC/MIT; Optical: NASA/STScI). Right panel: optical image of cluster Abell 1914 from the Sloan Digital Sky Survey with the superimposed map of the temperatures of the Cosmic Microwave Background observed by the Sunyaev-Zeldovich array (SZA). The image illustrates the effect of up-scattering of the CMB photons by the hot ICM from low frequencies to higher frequencies. At the frequency of observation, the cluster appears as a temperature decrement in the CMB temperature map. (Credit: John Carlstrom and SZA collaboration).
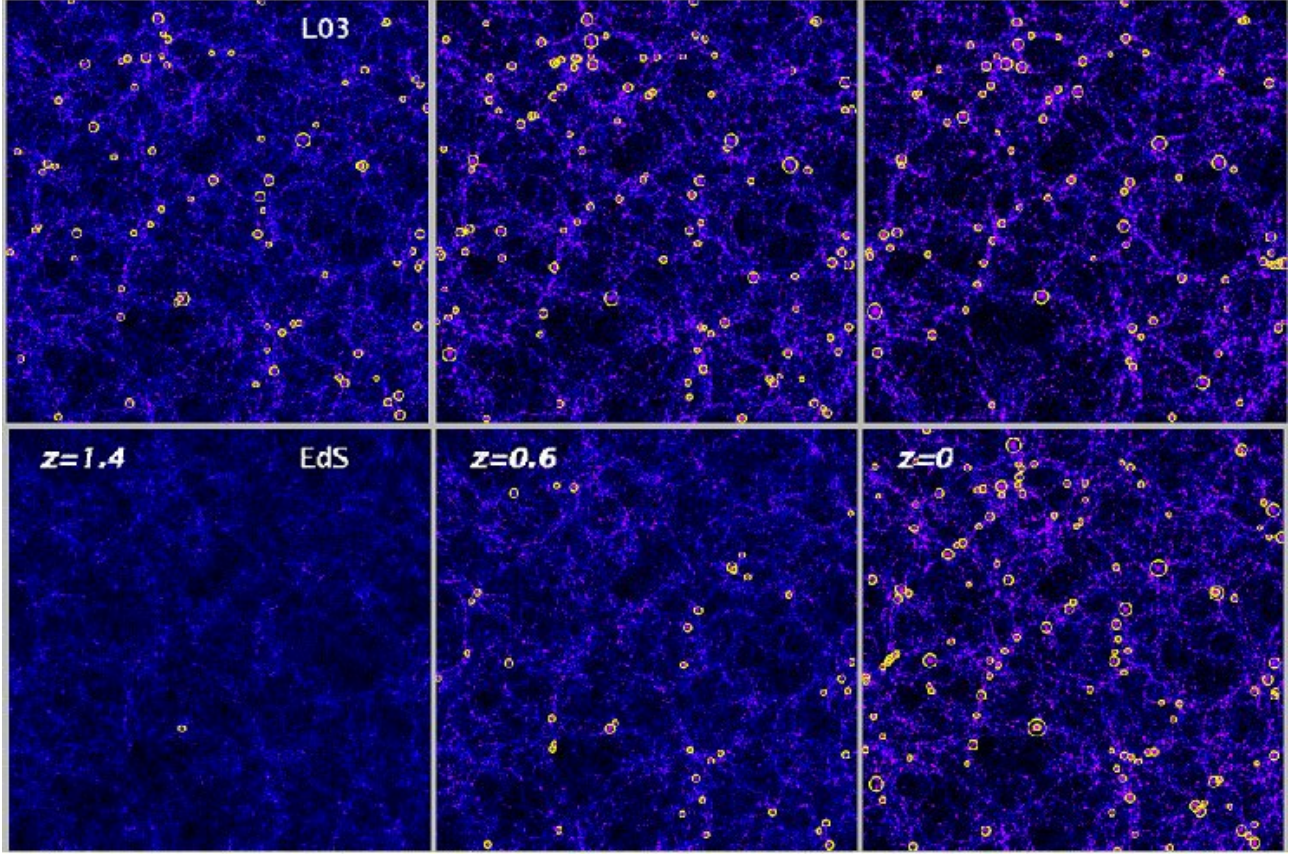
Figure 2: Evolution of large-scale cosmic structures simulated in N-body simulations of two different cosmological models. Each of the three redshift snapshots shows a region with $250\,h^{-1}$Mpc side and $75\,h^{-1}$Mpc thick (co-moving scale-lenghts). The upper panels describe a flat low–density model with $\Omega_{\rm m} = 0.3$ and cosmological constant contribution to the energy density of $\Omega_\Lambda = 0.7$, while the lower panels are for another spatially flat cosmological model with $\Omega_{\rm m} = 1$. In both cases the amplitude of the power spectrum is consistent with the number density of nearby galaxy clusters. Superimposed on the matter distribution, the yellow circles mark the positions of galaxy clusters that would be seen shining in X–rays with a temperature $T > 3$ keV. The size of the circles is proportional to temperature. The difference in the evolution of cluster abundance in the two models illustrates the importance of clusters as probes of the dark matter and dark energy content of the universe. Figure adopted from Borgani & Guzzo (2001) with copyright permission from 2001 Nature Publishing Group.

geometrically flat cosmological models with low mean matter density, $\Omega_m < 1$, the cosmological constant starts to dominate the energy density of the universe and drive accelerating expansion at redshift $(1 + z) = \Omega_m^{-1/3}$ or $z \approx 0.5$ (e.g., Carroll et al., 1992). This example highlights the important role that galaxy clusters play in tracing the cosmic evolution and in constraining the dark matter and dark energy content of the universe.

At scales below 1 Mpc, the physics of baryons starts to play an important role in addition to gravity, thus significantly complicating the associated processes. As we describe in more detail below, in the current paradigm of structure formation clusters are thought to form via a hierarchical sequence of mergers and accretion of smaller systems driven by gravity and dark matter that dominates the gravitational field. During this sequence the intergalactic gas is heated to high, X-ray emitting temperatures by adiabatic compression and shocks, and settles in hydrostatic equilibrium within the cluster potential well. Once the gas is dense enough, it cools, leaves the hot phase, forms the stellar component and can accrete onto supermassive black

holes (SMBHs) harbored by the massive cluster galaxies. The process of cooling and formation of stars and SMBHs can then result in energetic feedback due to supernovae or active galactic nuclei (AGN), which can inject substantial amounts of heat into the ICM and spread heavy elements throughout the cluster volume.

Within this global picture, galaxy clusters represent the place where astrophysics and cosmology meet each other: while their overall dynamics is dominated by gravity, the astrophysical processes taking place at the galactic scale leave observable imprints on the diffuse hot gas (e.g., Voit, 2005). Indeed, the gravitational potential wells of massive clusters are extremely deep and clusters therefore are expected to contain a universal fraction of baryons within a suitably large radius[4]. Given that we can probe each of their components with observations, clusters are powerful laboratories where to study the processes operating during galaxy formation and their effects on the surrounding intergalactic medium. As we will discuss in the following sections, hydrodynamical codes coupled to N-body techniques represents the most advanced instruments to describe such complex processes and their impact on the assembly history of cosmic structures.

1.3   Theoretical models of galaxy clusters

1.3.1   The "spherical cow" model: self–similar clusters

Before we delve into the complexities of the numerical description of cluster formation, it is instructive to consider the simplest model, which provides a useful baseline for evaluation of more accurate and sophisticated models. Such a model assumes that cluster properties and correlations between them are determined by gravity alone and that clusters are in virial equilibrium (Kaiser, 1986, see Voit 2005 for a review). Since gravity does not have preferred scales, in this model we expect clusters to be *self-similar* (i.e., clusters of different mass to be the scaled version of each other) and their mass to be the only parameter that determines the thermodynamical properties of the intra-cluster gas.

If, at redshift z, we define M_{Δ_c} to be the mass contained within the radius[5] r_{Δ_c}, encompassing a mean overdensity Δ_c times the critical cosmic density at the redshift of observation $\rho_c(z)$, then $M_{\Delta_c} \propto \rho_c(z)\Delta_c r_{\Delta_c}^3$. The critical density of the universe scales with redshift as $\rho_c(z) = \rho_{c0}E^2(z)$, where

$$E(z) \,=\, H(z)/H_0 \,=\, \left[(1+z)^3\Omega_m + (1+z)^2\Omega_k + \Omega_\Lambda\right]^{1/2} \tag{1}$$

gives the evolution of the Hubble parameter $H(z)$. In the above expression $\Omega_k = 1 - \Omega_m - \Omega_\Lambda$ is the contribution from curvature (we neglect here any contribution from relativistic species, e.g., Peebles, 1993). Therefore, the cluster size r_{Δ_c} scales with z and M_{Δ_c} as $r_{\Delta_c} \propto M_{\Delta_c}^{1/3}E^{-2/3}(z)$.

Given that the gas heated by gravitational infall is assumed to be in equilibrium within the gravitational potential Φ of the cluster, it is expected to have the temperature $k_B T \propto \Phi \propto M_{\Delta_c}/r_{\Delta_c}$ (k_B: Boltzmann constant). Therefore the above relation between radius and mass gives

$$M_{\Delta_c} \,\propto\, T^{3/2}E^{-1}(z)\,. \tag{2}$$

This simple relation between mass and temperature can be turned into scaling relations among other observable quantities.

As for the X-ray luminosity, it scales as the characteristic emissivity times the volume occupied by the cluster. If we assume that thermal bremsstrahlung process dominates the emission from

---

[4]As we discuss in § 4.4 below the observational picture is currently more complicated.

[5]Throughout this paper the subscript of the radius indicates either the overdensity which the radius encloses with respect to the critical density $\rho_c(z)$ at the redshift of observation (e.g. r_{500} is the radius enclosing overdensity of $500\rho_c$) or that the radius encloses the virial overdensity ($r_{\rm vir}$) predicted by the spherical collapse model (e.g. Eke et al., 1996).

the ICM plasma with electron number density n_e (e.g., Sarazin, 1986; Peterson & Fabian, 2006), we have $L_X \propto n_e^2 T^{1/2} r_{\Delta_c}^3$. The characteristic density scales as $n_e \propto M/r_{\Delta_c}^3 = \text{const}$ and $T \propto M_{\Delta_c}/r_{\Delta_c}$, which (using the $M - T$ relation above) gives $L_X \propto T^2 E(z)$.

Another useful quantity to characterize the thermodynamical properties of the ICM is the entropy (Voit, 2005). In X–ray studies of the ICM, it is usually defined as

$$S = \frac{k_B T}{\mu m_p \rho_{gas}^{2/3}} . \tag{3}$$

With the above definition, the quantity S is the constant of proportionality in the equation of state of an adiabatic mono-atomic gas, $P = S\rho_{gas}^{5/3}$. Using the thermodynamic definition of specific entropy, $s = c_V \ln(P/\rho_{gas}^{5/3})$ (c_V: heat capacity at constant volume), one obtains $s = k_B \ln S^{3/2} + s_0$, where s_0 is a constant. Another quantity, often called "entropy" in cluster studies, that we will also use in the following, is

$$K = k_B T n_e^{-2/3} . \tag{4}$$

According to the self–similar model, this quantity, computed at a fixed overdensity Δ_c, scales with temperature and redshift according to

$$K_{\Delta_c} \propto T E^{-4/3}(z) . \tag{5}$$

Self–similar X–ray scaling relations for the ICM are also predicted by the spherically-symmetric accretion model originally proposed by Bertschinger (1985). Supersonic accretion gives rise to an expanding accretion shock taking place at the interface of the inner hydrostatic gas with a cooler, adiabatically compressed, external medium. This model has been later generalized to include cooling of gas (with cooling functions of a certain form) (Abadi et al., 2000) and to include the effect of external pre–heating of the diffuse inter-galactic medium, still under the assumption of spherical accretion, as a way to break self–similarity (Tozzi & Norman, 2001; Voit et al., 2003).

The predictions of the self–similar model have been tested by a number of authors against hydrodynamical simulations, which include only the effect of gravitational heating (e.g., Navarro et al., 1995a; Eke et al., 1998; Nagai et al., 2007a). These simulations generally confirmed the above scaling relations for the overall average quantities and for the radial profiles, as well as their evolution with redshift, although small deviations from self–similarity, due to the differences in formation redshifts of systems of different mass and some small differences in the dynamics of baryons and dark matter have also been found (Ascasibar et al., 2006). As we shall discuss in § 4, however, the predictions of this model are at variance with respect to a number of X–ray observations, indicating importance of other physical processes in addition to gravitational heating.

1.3.2   Numerical simulations of cluster formation

The self–similar model and its more complicated spherically-symmetric extensions introduced in the previous section, while useful as a baseline for the interpretation of observations, are far too simple to capture all of the complexities of cluster formation (see § 3 and 4). As already mentioned, numerical cosmological simulations carried out on massive parallel supercomputers represent the modern instruments to describe these complexities. Such simulations start at a sufficiently early epoch when density fluctuations are still small and can be specified using early evolution models. The initial conditions are a realization of a density field with statistical properties[6] (e.g., the power spectrum) appropriate for the adopted background cosmological model.

---

[6]The initial density field is usually assumed to be Gaussian (see, however, Grossi et al., 2008; Dalal et al., 2008; Pillepich et al., 2008, for examples of non-Gaussian simulations), in which case it is fully specified by the power spectrum of fluctuations.

The numerical simulations follow the co-evolution of the collisionless dark matter component and normal baryonic matter, which interact only via gravity, starting from the initial conditions and advancing the density and velocity fields forward by numerically integrating equations governing the dynamics of dark matter and baryons.

A number of observational probes, such as the Cosmic Microwave Background, the statistics of the population of galaxies and galaxy clusters, the Hubble diagram of Type Ia supernovae, the pattern of gravitational lensing, and the properties of absorption systems in the spectra of distant quasars, have provided tight constraints on the underlying cosmological model (e.g., Komatsu et al., 2008, and references therein). This implies that initial conditions for cosmological simulations can now be fixed with a far lower degree of ambiguity than it was possible until ten years ago. Cosmological simulations are therefore quite "lucky" compared to many other areas of computational science in that the initial conditions are unique and well specified. The main challenge for the simulations is thus to faithfully follow dynamics of matter driven by gravitational instability and the gas-dynamical processes affecting the evolution of the cosmic baryons.

The dynamics of collisionless DM is described by the collisionless Boltzmann equation (also known as the Vlasov equation), which is the continuity equation of the fine-grained phase space density in the six dimensional space of coordinates and velocities. The high dimensionality of the phase space makes it extremely demanding to numerically solve the Boltzmann equation directly. Therefore, as is often the case in integrating equations of high dimensionality, the Monte Carlo technique is used. The solution to the Vlasov equation can be represented in terms of characteristic equations, which describe lines in phase space along which the distribution function is constant. These equations are identical to the standard Newtonian equations of particle motion. The complete set of characteristic equations is equivalent to the Vlasov equation. In cosmological simulations only a representative subset of characteristic equations is solved by discretizing and sampling the initial phase space by N particles ("bodies") and then integrating their equations of motion in the collective gravity field (equivalent to solving the characteristic equations).

Dynamics of diffuse baryonic matter is expected to be highly collisional (see § 4.3) and is therefore followed using standard hydrodynamics techniques. All of the matter components in a simulation interact with each other only via gravity. The integration of a coupled set of the governing equations allows one to provide information about matter properties in three dimensional space at different epochs.

Crucial parameters in defining the accuracy of a simulation are the mass and spatial resolution. The mass resolution is intuitive: it is simply the mass of the smallest mass element. Spatial resolution requires some explanation. Each particle or volume element in a simulation is assumed to have a certain shape (for example, a box or a sphere), size and internal density distribution. For the non-overlapping cells, used for example in the Eulerian hydrodynamics solvers, the spatial resolution is simply the size of the smallest cells. For collisionless dark matter particles or particle-based hydrodynamics solvers, in which particles can overlap, the resolution is the scale at which gravity and/or hydrodynamics forces are smoothed.

The mass and spatial resolution should be tightly related (e.g., Knebe et al., 2000; Power et al., 2003; Diemand et al., 2004), but are not always identical in the actual simulations (e.g., high mass resolution in a simulation with low spatial resolution does not necessarily mean that the smallest mass elements are faithfully followed). Ideally, increasing the number of particles and fluid elements employed to describe the dynamics should lead to convergence to the true solution. In practice, however, the convergence can be slow and the convergent solution may deviate from the true solution because discretized versions of equations solved in simulations are different from the real equations (e.g., due to the addition of extra terms related to numerical viscosity, etc.).

The first simulations of cluster formation have been performed in the 1970s and 1980s (Peebles, 1970; White, 1976) and were instrumental in testing the general idea of gravitational instability as

the driving process of cluster formation. The first simulations of galaxy clusters, which followed the dynamics of both baryons and dark matter, were carried out during the late 80s and early 90s (Evrard, 1988, 1990; Thomas & Couchman, 1992; Katz & White, 1993; Bryan et al., 1994; Kang et al., 1994; Navarro et al., 1995a). Many of these pioneering simulations have assumed that radiative losses of the diffuse gas can be neglected, since cooling time for the bulk of the gas is longer than a typical cluster age or even the age of the universe.

The addition of baryonic component has allowed simulations to predict properties of clusters observable in X-rays, as they confirmed that gas was heated to X-ray emitting temperatures during cluster formation via adiabatic compression and shocks. These early simulations were quite successful in reproducing general morphological characteristics of the X-ray observations available at the time. The simulations have also showed that gas in the inner regions of clusters is in approximate hydrostatic equilibrium and have confirmed the expectation from the simple models that their X-ray observables are tightly correlated with the total cluster mass (Evrard et al., 1996). These advances provided a foundation for the use of clusters as probes of cosmological parameters. Further progress in simulations and observations has shown that details of cluster formation and physics are more complicated and involve effects related to formation end evolution of cluster galaxies. While the outer regions of clusters, at radii larger than about 10 per cent of the virial radius, are quite regular, nearly self-similar, and are well described by simulations, the inner core regions exhibit large scatter and evidence of galaxy formation effects and energy injection by the central AGN. Studies of these effects have blossomed into an active and vibrant field of research. We review the numerical modeling aspect of this field in the following sections.

2   Techniques of cosmological simulations of cluster formation

As we mentioned in the previous section, cosmological simulations of cluster formation are started from the initial density field at an early epoch, when the typical matter density fluctuations around the cosmic mean density are small ($\delta\rho/\rho < 0.3$) at the smallest resolved scales[7]. The fiducial assumption is that the density field is Gaussian with a power spectrum of fluctuations that can be exactly computed for the assumed cosmological model (see, e.g., Seljak et al., 2003). The field is evolved to the chosen initial epoch using a model sufficiently accurate to describe the evolution of fluctuations in linear and mildly non-linear regime, such as the Zeldovich approximation (Zel'dovich, 1970; Klypin & Shandarin, 1983; Efstathiou et al., 1985, for recent reviews see Sirko 2005 and Prunet et al. 2008) or higher-order perturbation theory (e.g., Crocce et al., 2006).

In cosmological simulations, gravitational forces acting on both dark matter and baryons and hydrodynamics forces acting only on baryonic matter are computed using different numerical schemes. For gravity, the most direct scheme is based on computing the force among each pair of particles. Although this direct integration scheme (e.g. Aarseth, 2001) is in principle the most accurate, the required number of operations scales like the square of the total number of employed particles, thus making it prohibitively expensive for large cosmological simulations. For this reason, different schemes have been developed to trade between computational speed and numerical resolution or accuracy. Such schemes include grid-based particle-mesh (PM) and particle-particle/particle-mesh (P^3M) methods (Hockney & Eastwood, 1988; Couchman, 1991), the gridless tree method where forces are computed by multipole expansion (Barnes & Hut, 1986; Bouchet & Hernquist, 1988), or a hybrid of the two methods with the fast PM scheme

---

[7]The scale is comparable to the mean interparticle separation

used to compute gravitational forces on large scales and the tree algorithm to compute forces on smaller scales (Bagla, 2002; Bode & Ostriker, 2003; Springel, 2005). The PM methods solve the Poisson equations discretized either on uniform or non-uniform grids (e.g. in the Adaptive Mesh Refinement methods) using FFT method or a multi-grid relaxation solver. Each particle is treated as a cubic volume element with a specified inner density distribution when its density is interpolated onto the grid for the Poisson solver. Gravitational forces are usually computed by finite differencing the potential produced by the Poisson solver and are used to advance particle positions and velocities or update baryon variables in a grid cell.

As for hydrodynamics[8], the two most commonly used approaches are gridless smoothed particle hydrodynamics (SPH) and shock-capturing grid-based methods[9]. In the SPH, fluid elements describing the system are sampled and represented by particles, and the dynamic equations are obtained from the Lagrangian form of the hydrodynamic conservation laws (see Monaghan, 2005, for a recent review). The main advantage of SPH lies in its Lagrangian nature as there is no grid to constrain the dynamic range in spatial resolution or the global geometry of the modeled systems. However, in order to prevent particles from penetrating shock regions, the SPH scheme uses an artificial viscosity, which allows the kinetic energy of such particles to be converted into thermal energy. Clearly, the presence of an artificial viscosity term could prevent the development of shear motions, thus spuriously preventing the development of turbulent flows. This limitation of the SPH codes can be at least partially overcome by introducing suitable schemes to let artificial viscosity decay away from the shock regions (Morris & Monaghan, 1997; Dolag et al., 2005). Furthermore, SPH has a limited ability to describe strong gradients in thermodynamical variables (occurring, for example, in a multi-phase medium or during cluster mergers; Agertz et al. 2007) or low-density regions with a finite number of particles.

Modern grid-based shock-capturing methods (e.g., Laney, 1998) perform well for flows with shocks and contact discontinuities and for moderately subsonic and turbulent flows. These methods are typically capable of resolving shocks with just 1-2 grid cells and contact discontinuities on 3-5 cells. For given computational resources, shock-capturing codes can treat far more cells than the SPH codes can treat particles, but the cells are, in the case of a regular uniform grid, evenly spaced rather than concentrated into the more interesting high-density regions as occurs naturally in SPH codes. This is why in earlier studies the Eulerian schemes were used mostly for simulations of large-scale structures and clusters in large volumes (e.g., Cen & Ostriker, 1992; Kang et al., 1994; Bryan & Norman, 1998; Miniati et al., 2000), while SPH codes were most often used to study detailed structure of clusters and galaxies simulated in a relatively small volume (e.g., Evrard, 1990; Katz & Gunn, 1991; Thomas & Couchman, 1992; Katz & White, 1993; Evrard et al., 1994; Navarro et al., 1995b; Frenk et al., 1996; Yoshikawa et al., 2000). Examples of this are represented by the SPH cosmological simulations of formation of disk galaxies, which are resolved by several hundreds of thousands particles (see Mayer et al., 2008, for a review), and of galaxy clusters, currently resolved by up to tens of millions gas particles (e.g., Dolag et al., 2008a).

The situation has changed in the last ten years due to a wider adoption of adaptive mesh refinement (AMR) techniques for cosmological simulations (e.g., Norman & Bryan, 1999; Abel et al., 2000; Kravtsov et al., 2002; Teyssier, 2002; Loken et al., 2002), which make shock-capturing gasdynamics schemes competitive with the SPH. The AMR is used to increase the spatial and temporal resolution of numerical simulations beyond the limits imposed by the available hardware. This is done by using fine mesh only in regions of interest (such as high-density regions or regions of steep gradients in gas properties) and coarse meshes in other regions (low-density

---

[8]The validity of hydrodynamic treatment of intracluster plasma as an ideal fluid is a rather complicated issue, which we discuss in § 4.3.

[9]Other schemes, such as Godunov-type Particle Hydrodynamics (GPH; Inutsuka, 2002), Smoothed Lagrangian Hydrodynamics (SLH; Gnedin, 1995) and Adaptive Moving Mesh (Pen, 1998).
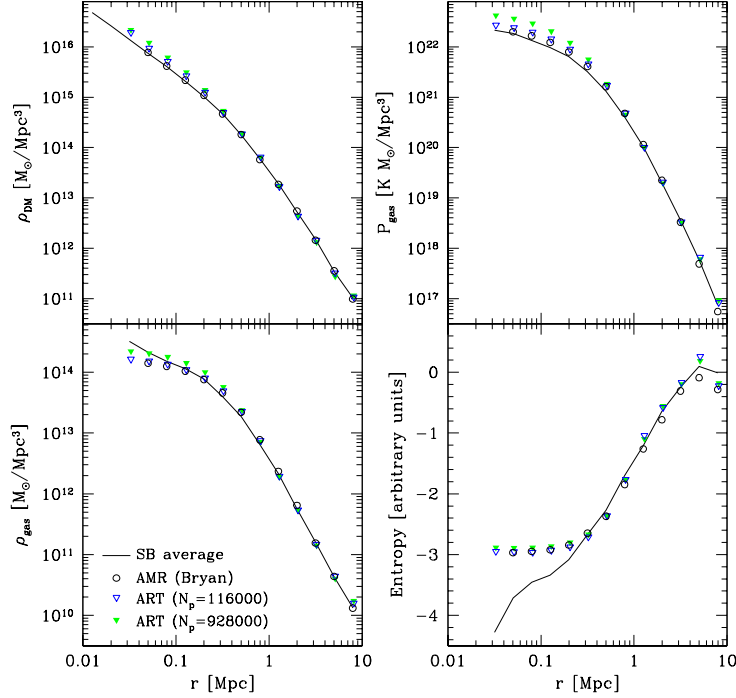
Figure 3: A comparison between profiles of dark matter density, gas density, gas pressure and gas entropy obtained by simulating the Santa Barbara (SB) cluster (Frenk et al., 1999) with different codes. Open and solid triangles are for simulations carried out with the ART code Kravtsov et al. (2002) using $\approx 116,000$ and $\approx 928,000$ particles within the virial radius, respectively. The solid lines show the corresponding mean profiles originally presented in the SB cluster comparison project (Frenk et al., 1999). The open circles show profiles from the adaptive mesh refinement (AMR) simulation by Greg Bryan performed as part of the SB project. Figure adopyed from Kravtsov et al. (2002) with copyright permission from 2002 IOP Publishing Ltd.

regions or smooth flows). If only a small fraction of the total volume is refined, as is commonly done in cosmological simulations, AMR results in substantial memory and CPU savings compared to the uniform grid of comparable resolution. The saved computer resources can be used to dramatically increase resolution where it is really needed. AMR simulations of the formation of the first stars in the Universe (Abel et al., 2000), which have reached a dynamic range in excess of 10^{10}, are an impressive illustration of this point.

It is also important to keep in mind that although different numerical schemes aim to solve the same sets of equations, the actual discretized versions solved in simulations are not the same. This can and does lead to differences in the numerical solution (Agertz et al., 2007; Tasker et al., 2008). This implies both that different techniques are useful and complementary in assessing possible systematic errors associated with a given technique and that such errors can only be identified in comparisons of simulations performed using different techniques.

An example of such comparisons is shown in Figure 3 (Kravtsov et al., 2002), where results of two independent AMR codes (which use different techniques for the Poisson and hydrodynamics solvers) are compared with results of a set of SPH simulations using the "Santa Barbara comparison cluster" (Frenk et al., 1999). The figure shows very good general agreement between the two AMR simulations. Outside the core of the cluster there is also good agreement between all simulations. However, in the central regions the entropy profiles of the two Eulerian mesh refinement simulations show the presence of a well-resolved core, while the mean profile of other simulations, dominated by the SPH simulations, continue to decrease monotonically with decreasing radius. The difference is due to different mixing properties of the codes. The gas in the Eulerian AMR

codes mixes efficiently and the entropy in the core is effectively homogenized. Mixing in the SPH simulations is absent, however, and the low entropy gas can survive and sink towards the center via convective instability (Mitchell et al., 2008). Mixing in SPH simulations can be increased by either explicitly including a dissipation term in the equations of hydrodynamics (e.g., Price, 2008; Wadsley et al., 2008) or by minimizing the degree of artificial viscosity, thereby increasing the amount of resolved turbulence (Dolag et al., 2005). The difference in entropy profiles is also smaller for the "entropy-conservative" formulation of SPH (see Fig. 1 in Ascasibar et al., 2003). More recently, Springel (2009) proposed a new hydrodynamic scheme which is based on an unstructured mesh computed using the Voronoi tessellation and moving with local fluid flow. Although inherently Lagrangian, this scheme computes hydrodynamic forces and mass flows across the mesh boundaries, thus providing the accuracy of Eulerian codes in describing discontinuities and improving the treatment of mixing with respect to SPH.

While simple non–radiative simulations require a relatively low resolution to provide stable predictions about the properties of the ICM, a reliable description of the processes of star formation, galaxy evolution and of the feedback effects on the diffuse inter–galactic and intra–cluster media is far more challenging, both from a computational and from a physical point of view. Simulations of cluster formation that aim to describe the effects of galaxy formation and of energy injection from supernovae and AGNs, include models for dissipative and heating processes affecting the baryonic components. These processes are included using phenomenological parametrization of the relevant physics in the right hand side of the hydrodynamics equations in the form of additional sink and source terms (Cen, 1992; Cen & Ostriker, 1992; Katz, 1992; Katz et al., 1996; Yepes et al., 1997). For example, the gas heated by large-scale structure formation shocks (see § 3.1 below), supernovae, or AGNs can be allowed to dissipate its thermal energy via cooling, which is included as a sink term in the energy equation. The cooling rates are calculated using local values of gas density, temperature, and (often) metallicity using either a cooling model of ionized plasma or pre-computed cooling rate tables (an example of such tables can be found in Sutherland & Dopita, 1993).

Modeling galaxy formation processes in cluster simulations is extremely challenging because capturing the cosmological environment within which galaxy clusters form requires sampling scales of few tens of comoving Mpc, while star formation and relevant gas-dynamical processes in galaxies occur down to the parsec scales. Therefore, these processes are modeled using phenomenological "sub-grid" models describing what occurs at the scales not resolved in simulations. The rate at which cold dense gas is converted into collisionless stellar particles, for example, is parametrized as a power law function of the local gas density. This rate is used to decrease the gas density and spawn new collisionless stellar particles with the corresponding mass (see Kay et al., 2002, for a review); dynamics of the stellar particles is then followed in simulations using the same algorithms as for the collisionless dynamics of dark matter. It is important to note that just as dark matter particles in a simulation are meant to sample characteristics of the collisionless Boltzmann equation and not represent individual DM particles, stellar particles in simulations are also samples of the stellar distribution and are not meant to represent individual stars. Each stellar particle is therefore treated as a single-age population of stars and its feedback on the surrounding gas is implemented accordingly. The feedback here is meant in a broad sense and, depending on simulations, may include UV heating, injection of energy and heavy elements via stellar winds and supernovae, and secular mass loss by stars. Parameterizations of these processes are motivated by either observations (e.g., SN energy feedback) or by stellar models (winds, mass loss). Inclusion of enrichment by heavy elements and tracking of their diffusion allows one to account for the metallicity dependence of gas cooling rates and to use metallicity distribution in the ICM as an additional constraint on the models by comparing it to the observed distributions (see Borgani et al., 2008, for a review).

3 Cluster formation within a cosmological environment

3.1 How do clusters grow?

In the hierarchical Cold Dark Matter models of structure formation, virialized systems of all masses form via a sequence of accretions and mergers of smaller objects. During this sequence the evolution of each of the three main components of clusters (dark matter, diffuse gas, and stars) is deeply interconnected with the others. The DM component drives the gravitational collapse and the hierarchical accretion of smaller systems. To first approximation, gas follows this accretion pattern. Figure 4 shows how the distributions of DM (upper panels), gas (central panels) and stars (lower panels) evolve across cosmic time inside the region forming a cluster, as predicted by a cosmological hydrodynamical simulation. The gas distribution generally traces the DM distribution, with its pressure support making it smoother below the Jeans length scale. Furthermore, stars form since early epochs within high density halos, where gas can efficiently cool over a short time scale, thus making their distribution quite clumpy. These density maps highlight the hierarchical fashion in which the formation of cosmic structures proceeds. At early epochs large numbers of small DM halos are already in place and their distribution traces the nodes of a complex filamentary structure of the cosmic web. As time goes on, these filaments keep accreting matter, while small halos flow along them, finally merging onto larger halos, placed at the intersection of filaments, where galaxy clusters form. By the present time (left panels) a rather massive galaxy cluster has formed at the intersection of quite large filamentary structures. The virialized region of the cluster hosts a large number of galaxies which survived mergers of their diffuse dark matter halos, and is permeated by a nearly spherical gas distribution, resembling the observational image shown in Figure 1.

In the case of galaxy clusters, the process of hierarchical merging and accretion is particularly energetic due to the large masses of systems involved and filamentary structures that surround them. Strong gravitational pull of the collapsing cluster region can accelerate dark matter and gas to thousands of kilometers per second. Such high-velocity gas flows are initially strongly supersonic, with Mach numbers $M \sim 10 - 1000$, as the gas in the low density regions is relatively cold (e.g. Miniati et al., 2000; Ryu et al., 2003; Pfrommer et al., 2006; Kang et al., 2007). The supersonic flow then undergoes a shock and converts most of the acquired kinetic energy into internal thermal energy. These circumcluster shocks convert tremendous amounts of energy, $\sim 10^{61} - 10^{65}$ ergs, which makes cluster formation the most energetic events since the Big Bang.

These processes are illustrated in Figure 5 (adopted from Nagai & Kravtsov, 2003), which shows maps of projected gas density (top) and entropy (bottom) around a forming cluster in a ΛCDM cosmological simulation at four different redshifts. The figure illustrates the complex dynamical processes accompanying cluster formation: accretion of clumps and diffuse gas along filaments, strong accretion and virial shocks both around cluster and surrounding filaments, weaker merger shocks within the virial shock of the cluster, and the complicated flow pattern of the ICM gas revealed by the entropy map. Between $z = 1$ and $z = 0.5$, the main cluster undergoes a nearly equal mass merger. More common are smaller mergers and accretion of groups along large-scale filaments. The mergers play an important role as they generate shocks which heat the ICM inside out and are responsible for the bulk of its thermalization (McCarthy et al., 2007b). Mergers and accretion flows also generate turbulent motions and ICM mixing (Norman & Bryan, 1999; Ricker & Sarazin, 2001; Nagai et al., 2003; Sunyaev et al., 2003; Dolag et al., 2005) and possibly magnetic fields (Roettiger et al., 1999). Recently, the shocks and temperature discontinuities accompanying cluster mergers have been detected in a number of clusters with sensitive X-ray observations by the *Chandra* satellite (see Markevitch & Vikhlinin, 2007, for a recent comprehensive review).

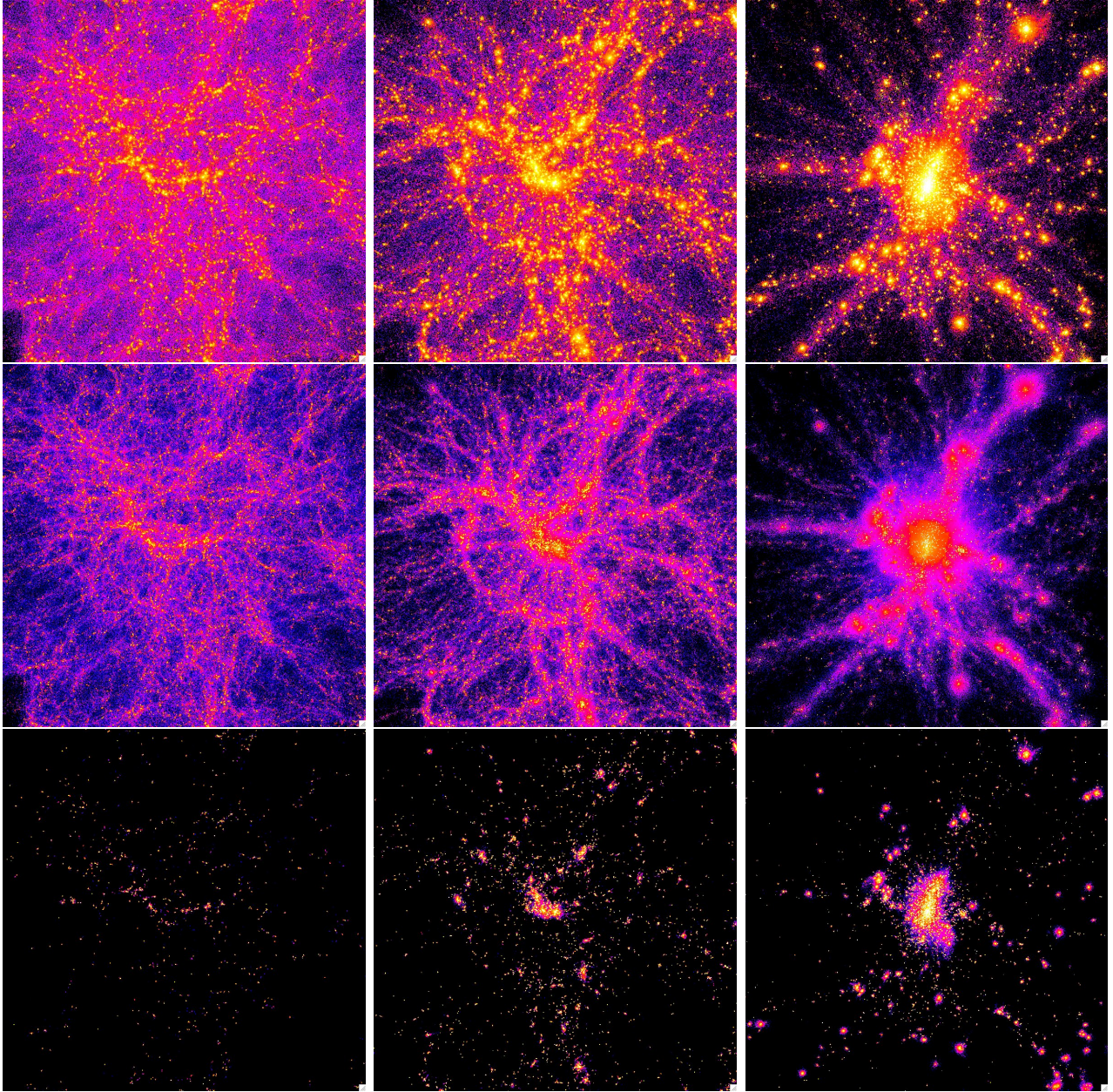The strong shocks discussed above are apparent as sudden jumps in entropy (from black to

Figure 4: The formation of a galaxy cluster in a cosmological context, as described by a hydro-dynamical simulation carried out with the Tree–SPH GADGET code (Springel, 2005). Upper, central and bottom panels refer to the density maps of dark matter, gas and stellar distributions, respectively. From left to right we show the snapshots at $z = 4$, where putative proto-cluster regions are traced by the observed concentrations of Lyman–break galaxies and Lyman–α emitters (e.g. Overzier et al., 2008), at $z = 2$, where highly star–forming radio–galaxies should trace the early stage of cluster formation (Miley et al., 2006; Saro et al., 2009), and at $z = 0$. This cluster has a total virial mass $M_{\rm vir} \simeq 10^{15} \, h^{-1} M_\odot$ at $z = 0$ (Dolag et al., 2008a). Each panel covers a comoving scale of about $24 \, h^{-1} {\rm Mpc}$, while the cluster virialized region at $z = 0$ is nearly spherical with a radius of about $3 \, h^{-1} {\rm Mpc}$.
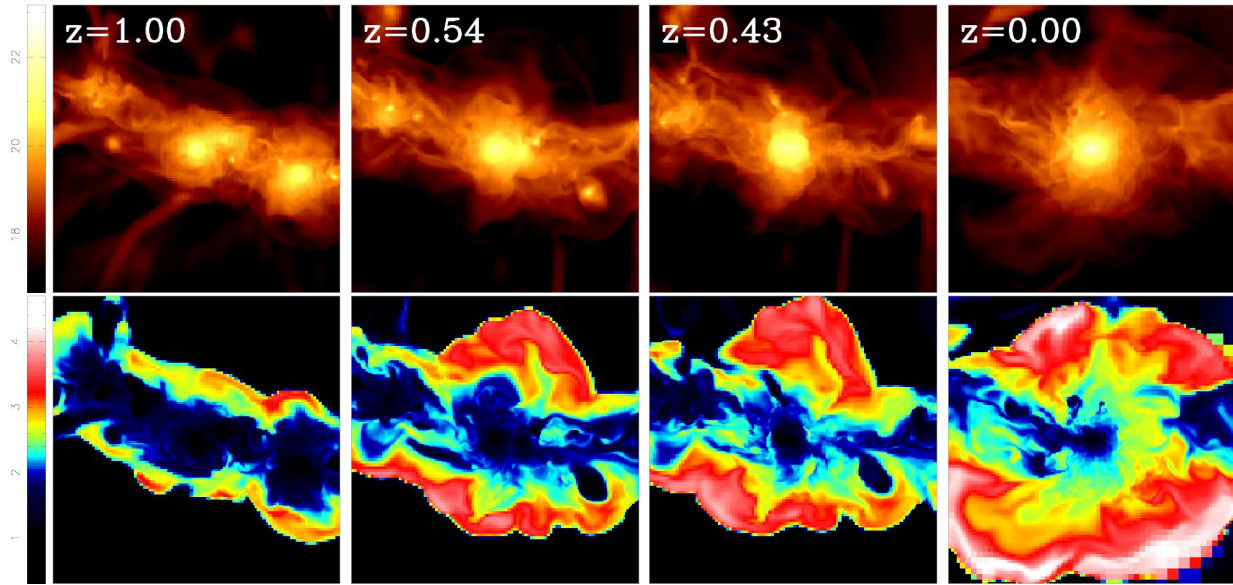
Figure 5: The maps of projected density (top) and entropy (bottom) of a simulated ΛCDM cluster at four different redshifts in a $60h^{-1}$ kpc slice centered on the central density peak. The maps are color-coded on a $\log_{10}$ scale in units of cm^{-2} (column density) and keV cm^2 (entropy). The size of the region shown is $8h^{-1}$Mpc. The maps reveal a very complex entropy distribution of the gas. Both the filaments and the forming cluster are surrounded by strong accretion shocks. Note, however, that the accretion shock around the cluster is very aspherical and does not penetrate into the filament; relatively low-entropy gas accreting onto cluster along the filament does not pass through the strong virial shocks and can be traced all the way to the central $0.5h^{-1}$Mpc of the cluster. Figure adopted from Nagai & Kravtsov (2003) with copyright permission from 2005 IOP Publishing Ltd.

color). The figure shows that accretion shocks have a non-trivial topology, as they surround both the merging clusters and the filament along which these clusters move. Note also that virial shocks do not penetrate into the filament itself and it is in fact difficult to separate the virial shocks of clusters from the accretion shocks around the filament.

During the evolution from $z = 1$ to $z = 0$, as the mass of the main cluster grows, the radius and entropy gradient of the virial shocks steadily increase. It is interesting that the virial radius, physically motivated by spherical collapse models, marks the transition from the inflow region, dominated by accreting material, to the relaxed part of the cluster only approximately (Eke et al., 1998; Cuesta et al., 2008). The quasi-spherical accretion shocks, for example, are generally located outside the virial radius at $\approx (2-3)R_{\mathrm{vir}}$ (right bottom panel in Figure 5).

Figure 5 shows that strong accretion shocks also exist and grow around the filament. Even at the present epoch the gas flowing along the filament reaches the central cluster regions without passing through a strong shock near the virial radius. This is clearly illustrated in the entropy maps in which relatively low-entropy gas flowing along the filament can be traced all the way to the central $0.5\,h^{-1}$Mpc of the cluster. The virial shocks instead propagate along directions of the steepest pressure gradient into the low-density voids. The flow of filamentary gas, with entropy already increased by the accretion shocks, has considerably smaller Mach numbers (typically $\sim 1-10$). When this gas reaches the cluster core it generates random, slightly supersonic motions in which it dissipates kinetic energy (see § 3.2 below).

3.2 Turbulence in the intracluster medium

The accretion flows described in the previous section and the motions of groups and galaxies, which perturb the surrounding medium by gravitational or hydro interactions, can generate substantial stochastic motions in the ICM. Energy of the large-scale turbulent eddies can cascade down to smaller scales resulting in power law turbulent energy and velocity spectra. In fact, numerical simulations of cluster formation generally show that subsonic random flows are ubiquitous even in apparently relaxed clusters (Norman & Bryan, 1999; Frenk et al., 1999; Nagai et al., 2003; Rasia et al., 2004; Kay et al., 2004; Faltenbacher et al., 2005; Dolag et al., 2005; Rasia et al., 2006; Nagai et al., 2007b; Lau et al., 2009).

Turbulence can have several important effects on the ICM. It can facilitate mixing of gas at different radii and correspondingly exchange of thermal energy, diffusion of heavy elements which would tend to broaden the centrally peaked abundance profile[10] (Rebusco et al., 2005). Viscous dissipation of turbulent motions can lead to secular heating of the ICM. Turbulence is also believed to maintain and amplify cluster magnetic fields via dynamo processes (Roettiger et al., 1999; Subramanian et al., 2006), and to contribute to the acceleration of cosmic rays in the ICM (e.g., Brunetti & Lazarian, 2007).

Quite importantly, incomplete thermalization of random gas motions can bias observational mass estimates of relaxed clusters, which rely on the assumption of hydrostatic equilibrium (HSE, e.g., Vikhlinin et al., 2006; Piffaretti & Valdarnini, 2008). Given that only thermal pressure is taken into account in the HSE analysis, the presence of random gas motions (or any other non-thermal pressure component) can contribute to the pressure support in clusters and bias HSE measurements of the total mass profiles (Evrard, 1990). Analysis of simulated clusters show that up to $\approx$ 10–20 per cent of pressure support comes from subsonic turbulent motions of gas (Rasia et al., 2004, 2006; Nagai et al., 2007b; Iapichino & Niemeyer, 2008). A recent comparison of mass from weak lensing and X-ray HSE mass measurement by Mahdavi et al. (2008) shows indeed that the HSE mass are lower by 10-20 per cent compared to lensing mass measurement, which may indicate the presence of turbulent (or some other non-thermal) pressure support in clusters.

Note that random motions not only bias the HSE mass estimates but also lead to a lower ICM temperature for a given total cluster mass, as part of the pressure support is contributed by the non-thermal pressure of random motions. The possible existence of these biases has important implications for the calibration and interpretation of scaling relations between total mass of clusters and their observable properties, such as the spectral X-ray temperature or the Sunyaev-Zeldovich signal. For instance, one can expect that random motions were even stronger in the past when the accretion and merger rate of clusters were higher, which would lead to certain evolution of normalization of the scaling relations. At a given epoch, the magnitude of the random motions increases with increasing distance from the cluster center and their effects can therefore be expected to be much stronger in the outskirts of clusters than in the core. A concentration of the total mass density profile derived from the HSE analysis would then be biased high, as the outer density profile would be derived to be steeper than it actually is. This may at least partially explain the high values of cluster concentrations derived in such analyses (Maughan et al., 2007; Buote et al., 2007).

How do simulation predictions on the ICM turbulence compare with observational data? The only tentative observational detection of ICM turbulence has been obtained from the spectrum of fluctuations in the pressure map from deep X–ray observations of the Coma cluster (Schuecker et al., 2004), which is consistent with those expected for a Kolmogorov spectrum. While future

---

[10]A strongly centrally concentrated metallicity profile can generally be expected because 1) the central regions of the cluster are strongly enriched by stars in the central galaxy and in the envelope surrounding it and 2) the ram pressure stripping of enriched interstellar medium of cluster galaxies is most effective in the cluster core where ICM density and galaxy velocities are large.

high resolution SZ observations will probe whether such pressure fluctuations are ubiquitous in most clusters, an unambiguous detection of stochastic motions would be obtained from direct measurements of gas velocities via X-ray spectroscopy (Inogamov & Sunyaev, 2003). The high spectral resolution required makes measurements challenging with the current X-ray instruments, while high–resolution spectrometers on the next generation X–ray satellites will open the possibility to infer the degree of ICM turbulence. As for simulations, the robustness of their predictions on ICM turbulence relies on their capability to correctly describe the physical viscosity of the gas, which is in turn affected by the presence of magnetic fields (see Sect. 4.3 below), and to have the numerical and artificial viscosity under control.

4   Making cluster simulations more realistic?

Although gravity is the main driver of galaxy clusters evolution, subtle but important effects on the properties of the ICM are expected from feedback processes related to star formation and accretion onto supermassive black holes. First unambiguous signature of these effects is provided by the detection of heavy elements, the so–called metals, within the ICM. Such elements are the product of stellar nucleosynthesis and chemically enrich the ICM at a level of about 1/3 of the solar value (e.g., Werner et al., 2008, for a review). This implies that gas–dynamical processes and galactic outflows should have transported and diffused metals from the interstellar medium, where they are released by SN, to the inter-galactic medium (Schindler & Diaferio, 2008, for a review).

Starting from the late 1980s, the availability of X–ray observations for statistically representative samples of clusters demonstrated that predictions of self-similar models are at variance with a number of observations. For instance, the observed luminosity–temperature relation (e.g., Markevitch, 1998; Arnaud & Evrard, 1999; Osmond & Ponman, 2004; Pratt et al., 2008) is significantly steeper than predicted, $L_X \propto T^\alpha$ with $\alpha \simeq 2.5$–3 at the scale of clusters and possibly even steeper for groups. Furthermore, the measured level of gas entropy in central regions is higher than expected (e.g., Ponman et al., 2003; Sun et al., 2008), especially for poor clusters and groups. Correspondingly, relatively poor systems were shown to have a relatively lower amount of gas (e.g., Vikhlinin et al., 2006; Croston et al., 2008), thus violating the basic assumption on which the self–similar model is based. This led to the notion that some physical process, besides gravity, should be responsible for the lack of self–similarity in the central regions of clusters and groups.

In the following sections we will review the attempts that have been undertaken over the last few years to incorporate effects of galaxy formation and of feedback energy release from supernovae and AGN into cosmological simulations of cluster formation. We will conclude with a discussion of the role played by a number of physical processes which are expected to take place in the ionized ICM plasma.

4.1   Cooling vs. heating the ICM with stellar feedback

The first mechanism introduced to break the ICM self–similarity is non–gravitational heating (e.g., Evrard & Henry, 1991; Kaiser, 1991; Tozzi & Norman, 2001). Early studies have suggested that observations can be explained if early ($z > 1$) pre-heating by galactic winds and/or AGNs injected significant amount of energy into the ICM (Kaiser, 1991; Evrard & Henry, 1991, see Voit 2005 for a review).

This entropy increase prevents the gas from sinking to the center of DM halos, thereby reducing gas density and X–ray emissivity. If E_h is the extra heating energy per gas particle, then this effect will be large for small systems, whose virial temperature is $k_B T \lesssim E_h$, while leaving rich

clusters with $k_B T \gg E_h$ almost unaffected. Therefore, we expect smaller systems to have a relatively lower gas fraction and X–ray luminosity, thus leading to a steepening of the L_X–T relation.

Cluster simulations in which the ICM was heated either via a model for supernovae-driven winds from cluster galaxies (Metzler & Evrard, 1994, 1997; Borgani et al., 2004; Davé et al., 2008) or via an arbitrary pre-heating at an early epoch (e.g., Navarro et al., 1995a; Mohr & Evrard, 1997; Bialek et al., 2001; Borgani et al., 2001, 2002; Muanwong et al., 2002, 2006) appeared to describe the observed X–ray scaling relations considerably better. Indeed, a suitable choice of extra energy and heating redshift can be eventually found, which produces the correct L_X–T relation. However, the amount of energy required to heat the ICM to the desired levels was too large to be provided by supernovae for a typical initial stellar mass function (Kravtsov & Yepes, 2000), even assuming high efficiency for the thermalization of supernovae-injected energy. Furthermore, an undesirable feature of pre–heating is that it creates fairly large isentropic core, thus at variance with respect to observational data showing a fairly low entropy level at the center of relaxed clusters (e.g., Donahue et al., 2006). Finally, observations of the statistical properties of the Lyα absorption lines in quasar spectra constrain any pre-heating to take place only in high density regions of the high-redshift intergalactic medium (Shang et al., 2007; Borgani & Viel, 2009).

Although it may look like a paradox, radiative cooling has been also suggested as a possible alternative to non–gravitational heating to increase the entropy level of the ICM and to suppress the gas content in poor systems. As originally suggested by Bryan (2000) and Voit & Bryan (2001), cooling provides a selective removal of low–entropy gas from the hot phase (see also Wu & Xue, 2002). As a consequence, only gas having a relatively high entropy will be observed as X–ray emitting. This analytical prediction is indeed confirmed by radiative hydrodynamical simulations (Pearce et al., 2000; Muanwong et al., 2001; Davé et al., 2002; Valdarnini, 2002, 2003; Kay et al., 2004; Nagai et al., 2007a; Ettori & Brighenti, 2008). Figure 6 shows a comparison between the entropy maps of the same cluster shown in Figure 4, simulated by including only gravitational heating (left panel) and radiative gas cooling along with star formation and chemical enrichment (which in turn affect the cooling rate; right panel). In the non–radiative case a number of merging subgroups show up as clumps of low-entropy gas within a high–entropy atmosphere, traced by the magenta/blue halo[11]. Due to the action of ram pressure, some of these clumps leave strips of low–entropy gas behind them, which form comet–like structures. This is quite apparent for the merging sub-halo located in the upper-right side with respect to the cluster center, which has just passed the apocenter of its orbit. This picture drastically changes in the radiative run. In this case, the removal of low entropy gas in the densest regions, including the core, has been so efficient that only relatively smooth structures are visible within the hot cluster atmosphere. A decrease in the density of the hot gas in central regions, as a consequence of cooling, is also shown in the left panel of Figure 7, where the gas density profiles in radiative and non-radiative simulations of this same cluster are compared.

Note that the dependence of the condensed gas fraction on cluster mass is weak (see § 4.4), thus cooling alone will not be able to break self–similarity to the observed level (see Figure 8). Furthermore, radiative cooling is a runaway process and converts too large a fraction of gas into stars. Indeed, observations indicate that only about 10-15 per cent of the baryon content of a cluster is in the stellar phase (e.g., Balogh et al., 2001; Lin et al., 2003; Gonzalez et al., 2007). On the other hand, the radiative simulation of the cluster shown in Figure 6 converts into stars about 35% of the baryons within the virial radius.

Another paradoxical consequence of cooling is that it increases the ICM temperature at the

---

[11]In the light of the discussion of Sect. 2, we expect that these low entropy clumps may partly evaporate in the presence of a mixing more efficient than that provided by SPH simulations.
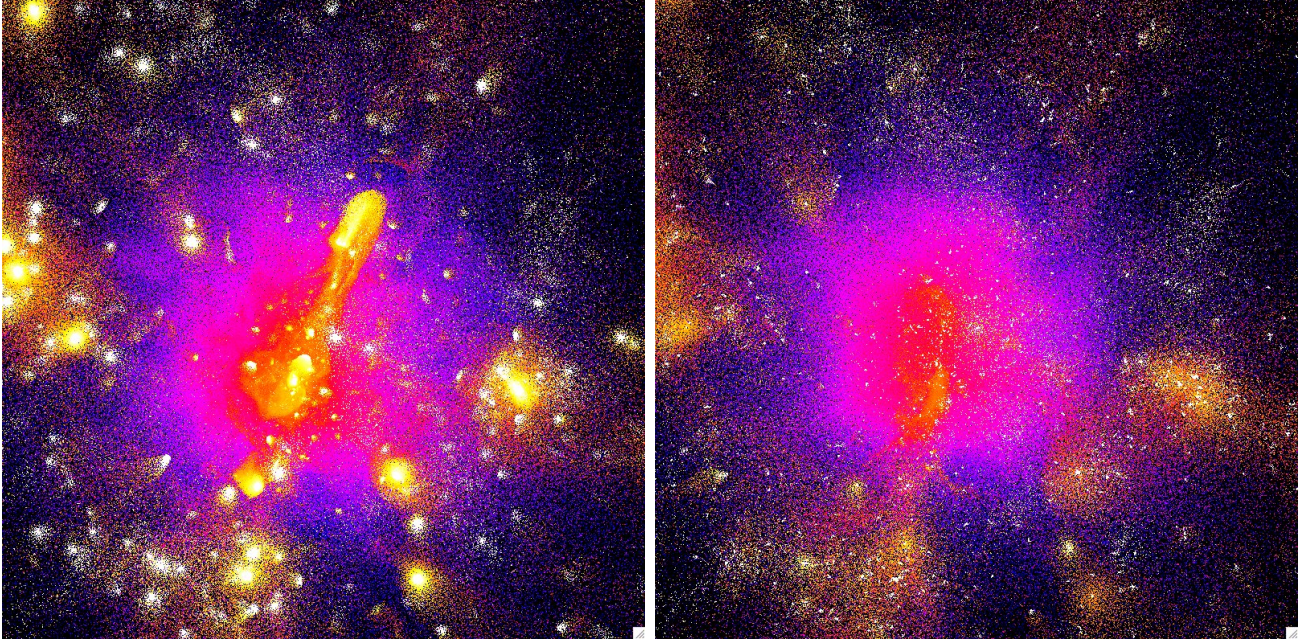
Figure 6: Maps of the gas entropy at $z = 0$ for the galaxy cluster shown in Figure 4, for the run with only gravitational heating (left panel) and for the run with cooling and star formation (right panel). Each panel encompasses a physical scale of about 8.5 Mpc. Brighter colors correspond to lower-entropy gas, while magenta and blue colors mark gas at progressively higher entropy. The simulations have been carried out with the Tree-SPH GADGET-2 code (Springel, 2005). The radiative simulation also include a description of chemical enrichment and the dependence of the cooling function on the gas metallicity (Tornatore et al., 2007).
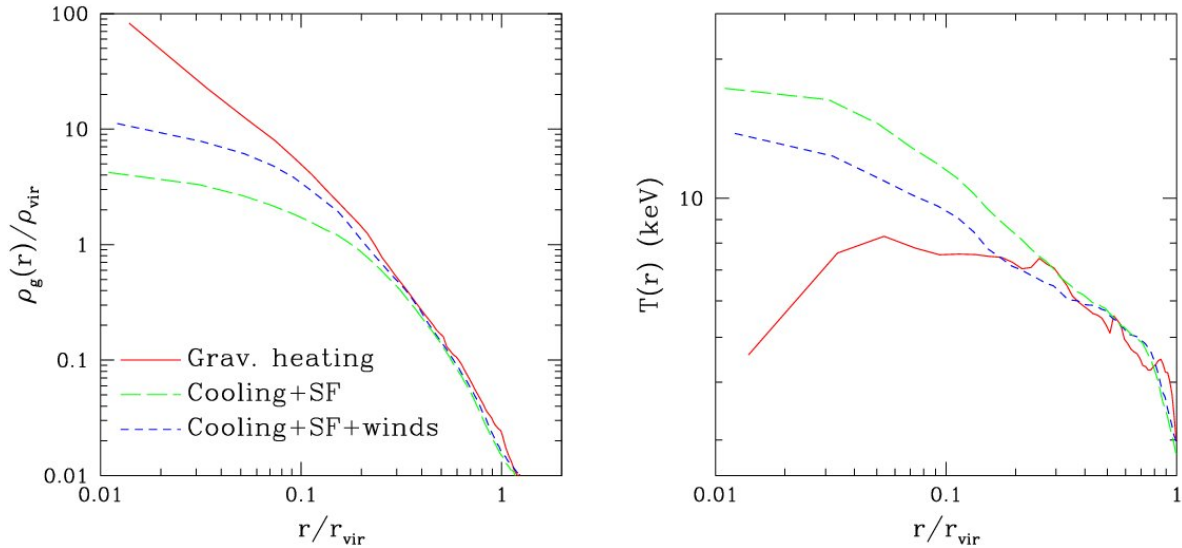

Figure 7: Comparison of the gas density (left panel) and temperature (right panel) profiles at $z = 0$ for the galaxy cluster shown in Figure 4. The three curves are for the run with only non–radiative physics (solid red), with cooling and star formation (long–dashed green) and also including the effect of galactic outflows powered by SN explosions (Springel & Hernquist, 2003a, long–dashed blue).

center of clusters. This is shown in the right panel of Figure 7 which compares the temperature profiles for the radiative and non–radiative simulations of the same cluster. The effect of introducing cooling is clearly that of steepening the temperature profiles at $r \lesssim 0.3 r_{\rm vir}$. The reason for this is that cooling causes a lack of central pressure support. As a consequence, gas starts flowing in sub-sonically from more external regions, thereby being heated by adiabatic compression. This steepening of temperature profiles represents another undesirable feature of simulations including radiative cooling.

As already discussed in the introduction, cosmological simulations of clusters are remarkably successful in reproducing the observed declining temperature profiles outside the core regions (e.g., Loken et al., 2002; Roncarelli et al., 2006), where gas cooling is relatively unimportant. This is illustrated in the left panel of Figure 9, which shows the comparison temperature profiles from clusters simulated with the SPH GADGET code (Borgani et al., 2004) and from a set of clusters observed with the XMM satellite. Quite apparently, simulated and observed profiles agree with each other outside the cool core regions. On the other hand, a number of analyses have demonstrated that radiative simulations fail at reproducing the observed gentle decline of temperature profiles in the core regions (e.g., Tornatore et al., 2003; Valdarnini, 2003; Nagai et al., 2007a). The left panel of Figure 9 shows the comparison between simulated and observed temperature profiles, based on a set of clusters simulated with the AMR ART code (Nagai et al., 2007a). This plot clearly shows that the central profiles of simulated clusters are far steeper than the observed ones, by a larger amount when cooling and star formation are turned on.

An eye-ball comparison with the right panel of Figure 7 shows a significant difference of the profiles in the central regions for the non–radiative runs. While SPH simulations predict a flattening, or even a decline, of the temperature profiles at $r \lesssim 0.1 r_{vir}$, Eulerian simulations are characterized by negative temperature gradients down to the smallest resolved radii. As already discussed in § 2, this difference is due by the lower degree of mixing and small–scale dissipation in SPH codes, with respect to Eulerian codes. As expected, including cooling provides an extra amount of dissipation, thus reducing the difference between the two hydrodynamical methods. Clearly, this further calls for the need of performing detailed comparisons between different simulation codes, for both non-radiative and radiative simulations, so as to have under control the reason for these differences.

Steepening of the central temperature profiles and overcooling are two aspects of the same problem. In principle, its solution should be provided by a suitable scheme of gas heating which compensates the radiative losses, pressurizes the gas in the core regions, and regulates star formation. Indeed, reproducing the observed star formation rate represents a challenge not only for cluster simulations, but more in general for simulations aimed at describing galaxy formation in a cosmological framework. Energy feedback from supernova explosions has been originally proposed to generate a self–regulated star formation. However, the physical processes which lead to the thermalization of the SN energy clearly require a sub–resolution description. This is a typical case in which the detail of the sub–resolution model leads to rather different results at the resolved scales. In Figure 7 we also show the effect of including a kinetic form of energy feedback, in the form of galactic outflows powered by SN explosions. This feedback mechanism was originally introduced with the purpose of producing a realistic cosmic star formation rate (Springel & Hernquist, 2003b). Therefore, it is in principle a good candidate to regulate gas cooling in cluster cores. The effect of this feedback is to partially compensate radiative losses and pressurize relatively low-entropy gas, which can now remain in the hot phase despite its short cooling time. If compared with the radiative run with no kinetic feedback, the temperature profile is somewhat flattened, gas density increases by more than a factor of two in the central regions and the baryonic mass fraction in stars drops to about 20 per cent.

Although these results go in the right direction, the effect of stellar feedback is generally not considered the right solution to the riddle of cool cores. In the above example, the temperature

profile, although flatter, does not show the gentle decrease in the innermost region, which would be the signature of a cool core (see the observed profiles in Figure 9). Furthermore, star formation rate in the BCG of this cluster is at a level of about 500 $M_\odot \text{yr}^{-1}$ (Saro et al., 2006), thus far larger than the few tens $M_\odot \text{yr}^{-1}$ indicated by observations (e.g., Rafferty et al., 2006). As a word of caution, we note that current cluster simulations are far from reaching high enough resolution to adequately describe the internal structure of galaxies and the multi-phase nature of the interstellar medium. Indeed, galaxy formation is still an open problem and it is not clear whether even simulations of single isolated galaxies, performed at much higher resolution (Mayer et al., 2008, for a review), are able to produce fully realistic objects. For this reason, the approach commonly followed is to explore a range of phenomenologically motivated models for star formation and SN feedback applied at relatively coarse resolution of cluster simulations (scales of $\sim 1-5$ kpc), rather than looking for the values of the parameters defining these models, which best reproduce the observational properties of galaxy clusters. Much work also remains to be done to explore sensitivity of the results to increasing resolution and inclusion of more sophisticated treatment of interstellar medium of galaxies.

More generally, the main observational motivation against stellar feedback as a mechanism to regulate star formation in cluster cores is that BCGs have a fairly old stellar population with a low star formation rate ("read and dead" galaxies). Therefore, they can not provide any significant source of feedback from SN explosions. As we shall discuss in the following, this calls for the need of introducing some sort of energy feedback, not directly related to star formation activity, the most popular candidate being represented by AGN feedback.

4.2 Modeling AGN heating in cluster simulations

Heating from AGN is due to energy released during accretion of the ICM gas onto a supermassive black hole harbored by the central cluster galaxy. Effects of AGN activity on the ICM are observed in many clusters (see McNamara & Nulsen, 2007, for a review) and the energy estimated to be injected by AGNs is sufficiently large to offset cooling and affect cluster gas in the core and beyond.

In particular, the AGN heating is thought to be the explanation for the puzzling absence of gas cooling in the central regions of dynamically relaxed clusters, the so-called "cool core" clusters. These clusters are characterized by a significant excess of X–ray emissivity due to the high density of gas in the center, which implies rapid radiative loss of thermal energy at such a high rate that all the gas in central cluster regions should cool to low temperature, $\sim 10^4$K, within a fraction of the typical clusters' age (e.g., Fabian, 1994). Yet, high-resolution X-ray spectra of core regions obtained during the past decade with the *XMM*-Newton and *Chandra* space telescopes do not show significant amount of gas at temperatures below $\sim 0.1-0.3$ of the virial temperature (see Peterson & Fabian, 2006, for a recent review). This implies the presence of steady heating within the cluster cores. AGN feedback is considered to be the most likely source of heating, due both to its central location and its ability to provide sufficient amounts of energy. The AGN heating is also thought to play an important role in quenching star formation in the brightest cluster galaxies, thereby reducing the cluster stellar mass fractions (see § 4.4). Trends of hot gas fractions and entropy in the inner regions with cluster mass also suggest AGN heating (e.g., Sun et al., 2008).

All of this shows the paramount importance of including the AGN heating in cluster simulations. The challenge, however, is that details of the heating mechanism are poorly understood. Some models show that episodic heating in the form of jets and bubbles does not result in a stable balance between cooling and heating, so that gas cooling is only delayed but not prevented (Vernaleo & Reynolds, 2006). This reflects a general difficulty to balance cooling or to prevent cooling instability. First, heating via an episodic jet may not be available in the specific

region where it is needed to offset the cooling, as a collimated jet can punch a narrow tunnel through the ICM gas and deposit its energy well away from the center. Second, even if the heat is distributed by some process, it does not guarantee stable balance between cooling and heating because cooling depends on the square of gas density, while heating generally depends on volume. Finally, the heating process, while offsetting cooling, should not increase the entropy significantly, as very low entropy gas is observed in the central regions of the cool core clusters (Donahue et al., 2006). The presence of such low entropy gas in core regions implies that this gas needs to be kept continuously pressurized by heating, so that it is prevented from cooling out of the hot X–ray emitting phase despite its formally short cooling time. The challenge is how to reach such a cooling/heating balance in a self-regulated way, without fine tuning the AGN duty cycle and the efficiency of energy thermalization.

Moreover, while entropy at small radii is observed to be surprisingly low, at larger radii $(r \sim r_{500})$ it is larger than predicted by non-radiative simulations (Voit et al., 2005; Sun et al., 2008). Semi-analytical models predict that the elevated magnitude of entropy could in principle be explained by smoothing of the intergalactic medium resulting from strong heating at high red-shifts (Voit & Ponman, 2003). However, it is not clear whether such predictions are confirmed by pre-heated simulations which also include radiative cooling (Borgani et al., 2005; Younger & Bryan, 2007) or whether they could also explain the observed nearly self-similar correlation of entropy at r_{500} with the overall cluster temperature (Nagai et al., 2007a). Heating by both AGN and galactic winds in general is not expected to scale linearly with cluster mass because AGN heating depends on the thermal processes and black hole mass on very small scales, while galactic winds heating should be a function of total stellar mass in the cluster, which does not scale linearly with cluster mass.

Keeping these challenges in mind, it is still clear that AGN heating in some form needs to be included in simulations of cluster formation for them to reproduce the observed properties of cluster core regions and ICM properties in smaller clusters and groups of galaxies. During the last several years, significant theoretical effort was dedicated to developing models of AGN heating of the ICM (Churazov et al., 2001; Quilis et al., 2001; Ruszkowski & Begelman, 2002; Brighenti & Mathews, 2003; Brüggen & Kaiser, 2002; Omma & Binney, 2004; Omma et al., 2004; Ruszkowski et al., 2004; Reynolds et al., 2005; Vernaleo & Reynolds, 2006; Cattaneo & Teyssier, 2007). All of these models, however, considered AGN activity outside the cosmological context of cluster formation. Although justified by the short time scale of a single heating episode, $\sim 10^8$ yr, one expects that cool core should be established at rather high redshift, $z \gtrsim 2$, when the inter-galactic medium starts reaching high enough densities around forming proto-BCGs. The overall effect of many different episodes both in the center of the cluster and in all of its progenitors can only be estimated by incorporating the AGN feedback in a full cosmological simulation.

First such simulations have recently been carried out (Sijacki et al., 2007; Bhattacharya et al., 2008; Sijacki et al., 2008). Based on the model for the SMBH formation and growth by Di Matteo et al. (2005), Sijacki et al. (2007) developed a model for AGN feedback via hot thermal bubbles in a full cosmological simulation of cluster formation (see also Puchwein et al. 2008). Several of the results (e.g., the relation between X–ray luminosity and temperature and the stellar fractions) from the simulations with AGN heating show a substantial improvement. However, this heating produces central entropy profiles inconsistent in both amplitude and shape with observed profiles exhibiting very low entropy in the inner 100 kpc (Donahue et al., 2006). More recently, Sijacki et al. (2008) have extended the model to include the injection of relativistic cosmic rays (CRs) in the AGN-blown bubbles. Interaction of cosmic rays with ICM provides a different buoyancy of the bubbles and a more steady source of heating as their dissipation rates are slow. As a result, CR heating can successfully regulate cooling flow and can significantly reduce stellar fraction in clusters. However, the resulting entropy profiles are still inconsistent with observations. This indicates that further improvements to the model will be needed to

reproduce detailed properties of ICM faithfully. Quite interestingly, Sijacki et al. (2008) also found that the non–thermal pressure support associated to cosmic rays can be as large as 50 per cent at the cluster center. This additional non-thermal pressure allows the gas to have declining temperature profiles towards the center without actually cooling. These results, as well as results of the CR effects in more idealized models of clusters (Boehringer & Morfill, 1988; Rephaeli & Silk, 1995; Mathews & Brighenti, 2007; Guo & Oh, 2008; Ruszkowski et al., 2008; Rasera & Chandran, 2008), indicate that cosmic rays are likely an important component of the ICM physics.

The presence of relativistic electrons is also suggested as a likely explanation for the observed soft (e.g., Werner et al., 2007) and hard (e.g., Sanders & Fabian, 2007) excess in the core of few clusters. In particular, Sanders & Fabian (2007) concluded from Chandra data that about 40 per cent of the electron pressure at the center of the Perseus cluster may have non-thermal origin. However, this conclusion has not been confirmed by the XMM observations by Molendi & Gastaldello (2009), who placed instead stringent upper limits to any hard excess in the X–ray spectrum from the core of Perseus. Furthermore, Churazov et al. (2008) derived an upper limit of 10–20 per cent to the non-thermal pressure in the core regions of two clusters, by combining X–ray and optical data. There is no doubt that the combination of observations at radio (e.g., Cassano et al., 2008), optical, X–ray and γ–ray (Perkins et al., 2006; Aharonian & the HESS collaboration, 2008) frequencies will allow us to understand the role played by cosmic rays play in cluster cores and, therefore, whether they need to be carefully modeled in cosmological simulations of clusters.

4.3   Modeling other physical processes in the intracluster plasma

Althoug almost all cosmological simulations discussed in the previous section treat intracluster plasma as an ideal inviscid fluid, the actual detailed processes in the ICM can be quite a bit more complex. On the one hand, the Debye screening length in the ICM is short ($\lambda_D \sim 10^7$ cm) and the number of particles within λ_D is large. The plasma can thus be treated as a neutral, continuous field on the scales resolved in cosmological simulations ($>$ kpc$= 3.0856 \times 10^{21}$ cm). On the other hand, the weakness of the Coulomb interactions means that, in the absence of magnetic field, the mean free path of the electrons is quite large: $\lambda_e \approx 23\,\mathrm{kpc}(T_e/10^8\,\mathrm{K})^2(n_e/10^{-3}\,\mathrm{cm}^{-3})^{-1}$ (e.g., Spitzer, 1962; Sarazin, 1986). For the typical conditions in the cluster outskirts, $T \sim \mathrm{few} \times 10^7$ K and $n_e \sim 10^{-4}\,\mathrm{cm}^{-3}$ at r_{500} (e.g., Vikhlinin et al., 2006), this mean free path can be as large as ~ 100 kpc, and the plasma formally cannot be considered as a strongly collisional gas on the scales resolved in simulations.

One can then ask whether the hydrodynamic treatment is at all reasonable. The answer is "yes" for two reasons. First, even a small, dynamically unimportant magnetic field can shorten the mean free path of the electrons significantly, at least in the direction orthogonal to the field line. Magnetic fields are indeed observed in cluster cores (e.g., Eilek & Owen, 2002; Carilli & Taylor, 2002) and there is a body of indirect evidence of their existence throughout the cluster volume (e.g., Carilli & Taylor, 2002; Govoni & Feretti, 2004; Eilek et al., 2006; Markevitch & Vikhlinin, 2007). In addition, magnetic fields are also predicted to be effectively amplified from the primordial values in mergers during cluster formation (Roettiger et al., 1999; Dolag et al., 1999, 2002; Schindler, 2002; Brüggen & Hoeft, 2006; Subramanian et al., 2006; Dolag & Stasyszyn, 2008). The questions are only how dynamically important the magnetic fields actually are, the actual magnitude of the mean free path suppression (which depends on the topology of the magnetic fields, see related discussion of conductivity below), and whether magneto-hydrodynamic effects are important in the ICM. In fact, MHD cosmological simulations suggests that magnetic fields generally provide a minor contribution to the total pressure (Dolag et al., 2001), while they can become dynamically non-negligible in peculiar cases involving strong mergers (Dolag & Schindler, 2000) or in strong cooling flows (Dubois & Teyssier, 2008).

Second, from plasma experiments (as well as observations of supernova remnants) it is clear that real plasmas exhibit a variety of excitation modes, in which electrons and ions move collectively in a correlated fashion. Fluctuations of the electromagnetic field generated by such motions appear to be much more efficient in scattering individual electrons than the Coulomb interactions. This means that the actual mean free path can be much smaller than the value for the Coulomb scatterings in unmagnetized plasma, at least in regions such as shocks, where deviations from local thermodynamic equilibrium are significant. This and the expected presence of magnetic fields probably make the use of hydrodynamic treatment of gas in cluster simulations justified.

Nevertheless, it is definitely worth investigating possible effects and ramifications of the breakdown of hydrodynamic limit. One approach is to treat the gas as a continuous fluid, but with kinetic perturbative correction terms to be added to the Vlasov equation, so as to account for the "rarefied" nature of the gas (Spiegel & Thiffeault, 2003). The collisionless effects and deviations from the collisional equilibrium can also be treated via explicit modeling of separate kinetics of electrons and ions (Chieze et al., 1998; Teyssier et al., 1998; Takizawa, 1999; Yoshida et al., 2005).

Whether the ICM can be treated as an inviscid fluid, as is done in most cosmological simulations of clusters, is a different question. Transport processes can be efficient and important for thermodynamics in clusters (see, e.g., Sarazin, 1986, for a review). Some amount of viscosity is introduced in the codes for numerical reasons, but this *artificial* viscosity, although important by itself (see, e.g., Dolag et al., 2005, for detailed discussion), should be distinguished from the real physical viscosity. The latter, however, is another factor that can affect important processes in the ICM, such as ram pressure stripping, dissipation of sound waves and random gas motions, survival of AGN bubbles. Sijacki & Springel (2006) have investigated the effect of adding the Spitzer–Braginskii physical viscosity (in addition to the numerical artificial viscosity), by implementing an SPH formulation of the Navier-Stokes equation. They find that the contribution of the physical viscosity is important and results in additional source of entropy due to viscous dissipation of motions generated by mergers and accretion accompanying cluster formation. Adding physical viscosity also makes ram pressure stripping of gas from infalling groups and galaxies more efficient (although see Roediger & Brüggen, 2008) and changes the morphology and disruption of the AGN-inflated bubbles. Since this viscosity is related to the Coulomb mean free path of the ions, it can be efficiently suppressed by the presence of magnetic fields. Therefore, its detailed description requires in principle a self–consistent description of the intra-cluster magnetic field.

Heat conduction is another important transport process to consider, as was pointed out by a number of studies over the last twenty years (e.g., Tucker & Rosner, 1983), if the conductivity is close to the Spitzer (1962) value for unmagnetized plasma. This is because the ICM is not isothermal and temperature gradients exist both in the core and in the outer regions (see Figure 9). In the context of the cooling flow problem, efficient conduction could provide a way to tap a vast reservoir of thermal energy at large radii in clusters. The value of the actual conductivity is highly uncertain due to uncertainties in the plasma processes and topology of intracluster magnetic fields (Tribble, 1989; Chandran & Cowley, 1998; Narayan & Medvedev, 2001; Malyshkin, 2001). An efficient conduction tends to create an isothermal core (e.g., Dolag et al., 2004). However, even when the conduction is close to the maximum Spitzer value, it may not be sufficient to fix all the problems in cluster modeling by itself. In particular, due to strong expected temperature dependence of conductivity (e.g, the Spitzer conductivity κ_S scales with temperature as $\kappa_S \propto T^{5/2}$) it is impossible to offset radiative cooling in low mass clusters, even if the conductivity is sufficient to offset cooling in high mass clusters (Voigt & Fabian, 2004; Dolag et al., 2004). Furthermore, conduction enters in a saturation regime whenever the typical scale of a temperature gradient falls below the electron mean free path. Therefore, whenever radiative cooling takes over, conduction may not be efficient enough to compensate radiative

losses by a heat transfer across the interface between cold and hot gas phases. This is the reason why conduction has a minor effect in decreasing the stellar mass fraction in cluster simulations (Dolag et al., 2004). Conduction also requires fine-tuning (Bregman & David, 1988; Conroy & Ostriker, 2008) and the thermal equilibrium mediated by conduction tends to be unstable (Kim & Narayan, 2003), although the problem may be mitigated by the regulation of conductivity by MHD turbulence related to magneto-thermal instabilities (Balbus & Reynolds, 2008). It is interesting to note that heat transport can operate not only as a kinetic effect via plasma particle scatterings, possibly suppressed by the presence of magnetic fields, but also as a heat carried over significant range of radii by large-scale subsonic turbulent eddies (Cho & Lazarian, 2004). In this case, the conduction can be quite efficient and comparable to the Spitzer conductivity and would not sensitively depend on the presence and topology of magnetic fields.

A potentially important heating mechanism in the ICM could be wakes generated by supersonic galaxy motions (El-Zant et al., 2004), although this process alone may not solve the cooling flow problem (Kim et al., 2005; Kim, 2007; Conroy & Ostriker, 2008). Motions by galaxies and infalling groups can also be an important driver of turbulent motions (e.g., Kim, 2007) that affect transport processes and can viscously dissipate their energy thereby heating the ICM (Dennis & Chandran, 2005). Although galaxy motions are modeled in high-resolution hydrodynamics simulations of clusters (Faltenbacher et al., 2005; Nagai & Kravtsov, 2005; Macciò et al., 2006), the current resolution may not be sufficient to follow the formation of wakes and transport of energy properly. Further simulations of this process for realistic clusters are needed.

Due to space limitation, this is but a brief overview of the examples of physical processes that can influence various aspects of the ICM evolution, but are often neglected in cosmological simulations of cluster formation. A more in depth discussion of these processes can be found in a recent review by Dolag et al. (2008b). The main purpose of our overview here was to give a sense of the effects and, most importantly, to highlight the fact that some aspects of the ICM physics are still rather poorly understood. This means that as many checks of models against observations as possible are required to make sure the models are a reasonable description of reality. We discuss some examples of how to constrain the ICM physics using observations below.

4.4   Constraints from the baryon and gas fractions in clusters

Measuring the fraction of the total mass in baryons within clusters, f_b, is one of the most powerful means to measure the density parameters contributed by matter, Ω_m, and by dark energy. Once the value of the baryon density parameter, Ω_b, is known (e.g. from observations of the CMB anisotropies or from primordial nucleosynthesis arguments), then measuring f_b for nearby clusters turns into a measurements of the matter density parameter, owing to $\Omega_m = \Omega_b/f_b$ (e.g., White et al., 1993; White & Fabian, 1995; David et al., 1995; Ettori & Fabian, 1999; Roussel et al., 2000; Castillo-Morales & Schindler, 2003). This method is based on the assumption that clusters contain a cosmic share of baryons. Furthermore, since the gas fraction measured from X–ray observations depends on the luminosity distance at the cluster redshift, assuming that this fraction does not evolve turns into a geometrical cosmological test, which allows one to also constrain the dark energy content of the universe (e.g., Sasaki, 1996; Pen, 1997; Allen et al., 2002; Ettori et al., 2003; LaRoque et al., 2006; Allen et al., 2008). Owing to the previous discussion on the effects of cooling and heating on the distribution of baryons within clusters, one may wonder how well funded are the above assumptions. For instance, while cooling results in the condensation of baryons, heating prevents gas from sinking in the cluster potential wells, thus potentially changing the value of f_b in the cluster environment. Furthermore, since both gas cooling and heating rates are expected to change with time, the value of f_b may also evolve with time. While the baryon fraction test has provided convincing constraints on the value of Ω_m,

precision cosmology based on f_b measurements for distant cluster requires the above uncertainties to be controlled with good precision, even assuming that the total cluster mass can be perfectly known.

Furthermore, the overall fraction of mass in the hot ICM and in the stellar component can be used as a useful diagnostic of the heating and cooling processes discussed in the previous section. Given the depth of gravitational potential wells of clusters, the total mass in baryons within a suitably large radius is expected to be close to the mean mass fraction of baryonic matter in the Universe. Indeed, non-radiative cosmological simulations show that the baryon fraction is close to universal within the virial radius, and even at smaller radii down to about half of the virial radius ($\approx r_{500}$; Frenk et al., 1999; Kravtsov et al., 2005; Ettori et al., 2006, see also Figure 10). The actual value of the total baryon fraction, of the stellar and hot gas fractions individually, and their scalings with cluster mass can be used as indicators of the heating and cooling processes operating during cluster formation.

Figure 10 shows the total baryon (stars plus gas) and hot gas mass fractions of observed and simulated clusters (from the sample presented in Nagai et al., 2007a) in units of the universal mean value within different radii (r_{2500} and r_{500} correspond to about a quarter and half of the virial radius, respectively). The red triangles show the total baryon fraction in non-radiative simulations. There is no visible trend of the baryon fraction with cluster mass in these simulations (see also Crain et al., 2007). The actual values are slightly below the universal fraction because gas and dark matter exchange energy and angular momentum during cluster formation with gas assuming a somewhat more extended radial distribution than dark matter (Lin et al., 2006).

In contrast, the baryon fraction in simulations with cooling and star formation is larger than the universal fraction and there is some trend of f_{bar} to decrease with increasing cluster mass. The enhanced baryon fraction is due to the fact that when baryons cool and condense in the centers of halos, that merge to form a cluster, they become much more resistant to tidal stripping than the dark matter, which is relatively loosely bound and is spread out in extended halos. Thus, compared to the non-radiative case, the condensed baryons are able to reach the center of the cluster when massive halos merge while dark matter is stripped and is deposited at larger radii. This difference leads to an increase of the baryon fraction in the inner cluster regions. In fact, the right panel clearly shows that the baryon fraction in the annulus outside the core is not enhanced in runs with cooling, but is actually somewhat suppressed.

Almost all of the baryons in the simulations shown in Figure 10 are either in the hot X-ray emitting gas or in collisionless stellar particles, created out of cold condensed gas. Thus, the difference between the total baryon fraction (open circles) and the hot gas fraction (solid circles) in each panel gives the stellar mass fraction. It is clear that the stellar fractions within r_{500} in these simulations are large (35–60 per cent depending on halo mass and radius) compared to observational estimates of the stellar mass fractions in clusters ($f_* \approx 10 - 20$ per cent, Lin et al., 2003; Gonzalez et al., 2007). This discrepancy is the consequence of the overcooling problem discussed above (see § 4.1).

Note that the overcooling problem and the cool core problem in observed clusters, although perhaps related, are not necessarily the same (Bryan & Voit, 2005). The cool core problem is the *current* lack of cooling gas in the cores of clusters where cooling time should be short. This requires balancing the radiative losses by suitably heating the gas after the cluster potential well has formed, i.e. at relatively low redshift, $z \lesssim 1$. The overcooling problem in simulations is the problem of too high mass of cooled, condensed gas produced *over the entire formation history* of the cluster, including all of its progenitors. This problem is more serious as it requires heating throughout the evolution of the cluster and of its progenitors and in particular at high redshift ($z > 2 - 3$), where most of the cluster stars are born.

An additional puzzle is that the observed hot gas fractions (Vikhlinin et al., 2006; Zhang et al., 2006; LaRoque et al., 2006, see data points in Figure 10) are quite low and are in fact consistent

with the hot gas fractions in simulations with cooling. Taken at face value, the observational measurements of stellar and gas fractions imply that the baryon fraction in clusters is considerably smaller than the expected universal value (e.g. Ettori, 2003; McCarthy et al., 2007a). The open and solid purple squares in the figure show baryon and hot gas fractions in a re-simulation of one of the clusters, in which cooling was artificially switched off after $z = 2$ (i.e., in the 10 billion years of evolution). The stellar fraction in this simulation (the difference between open and solid points) is about a factor of two smaller than in the other runs with cooling. However, the hot gas fraction is correspondingly larger and is larger than the observed gas fractions. This means that suppressing the stellar fraction without heating the gas, so as to push a significant fraction of it outside r_{500}, is not a viable solution.

These considerations leave us with three possible options: 1) the stellar fraction is suppressed by a heating mechanism, which also causes a substantial decrease of the gas fraction (and, hence, of the total baryon fraction) considerably below the universal value; 2) observational estimates of stellar fraction are biased low by a factor of 2-3, or a significant fraction of baryons (~ 20–30 per cent) in clusters, either in the form of a diffuse stellar component (e.g., Murante et al., 2007; Gonzalez et al., 2007) or of warm gaseous phase, are missed in observations; 3) the hot gas fraction in simulations are actually larger, and the low values inferred from observations are biased low for some reason.

The first option is plausible given the expected heating by supernova-driven winds and AGNs. The challenge in this case is to explain how this heating can substantially reduce the gas fraction at large radii in massive clusters (where the amounts of required heat injection would be tremendous), while retaining a nearly self-similar scaling of entropy at large radii (see Figure 8). In addition, explaining the very weak dependence of the gas fraction on the total cluster mass within r_{500} and in the shell between r_{2500} and r_{500} (see Figure 10 and Sun et al., 2008) is likely to be a challenge.

A detailed discussion of the second option is outside the scope of this review. We simply note that at the present time there is no solid observational evidence for a large fraction of baryons missing in clusters.

The low bias in the measurements of hot gas appears to be unlikely if the collisionless effects in the ICM plasma are negligible, as detailed tests of observational analyses techniques used to estimate gas fractions in the modern X-ray data shows that the methods are quite accurate (Nagai et al., 2007b). In fact, if there are non-thermal sources of pressure support in clusters, such as cosmic rays or turbulent motions, observational estimates of hot gas fractions would be biased high (because hydrostatic mass estimates using the thermal pressure along would be biased low). However, collisionless effects (see § 4.3) and deviations from equilibrium in plasma, such as evaporation, can potentially lower the gas fractions or bias observational estimates (e.g., Loeb, 2007).

4.5 Constraints on the models from the observed galaxy population

Whatever the nature of the feedback mechanism that shapes the thermodynamical properties of the ICM, we expect that it leaves its imprint on the history of star formation and, therefore, on the optical properties of the cluster galaxy population. In turn, a crucial diagnostic to trace the past history of star formation within cluster galaxies is represented by the pattern of chemical enrichment of the ICM (e.g., Renzini, 1997). It has been known for over twenty years that the level of enrichment in heavy elements of the ICM is about one third of the solar value, thus demonstrating that a significant fraction of the intra-cluster gas has been processed by stars and then expelled from galaxies (e.g., Baumgartner et al., 2005). Thanks to the much improved sensitivity of the X–ray telescopes of the last generation, it is also well established that the ICM metallicity, i.e. the ratio between the mass in metals and the mass in hydrogen, is not uniform.

Rather it is enhanced in correspondence of the cool cores (De Grandi et al., 2004; Vikhlinin et al., 2005; Baldi et al., 2007; Snowden et al., 2008; Werner et al., 2008; Leccardi & Molendi, 2008), where it reaches values comparable to solar. This enhancement is generally interpreted as due to the contribution to the enrichment from the past history of star formation in the BCG, thus highlighting the interplay between galaxy evolution and properties of the ICM.

How can we properly model the process of metal enrichment and connect it to star formation? Models of stellar evolution predict that SNe of different types (i.e. SN-II and SN-Ia) arise from stars of different mass, which explode over different time scales, and synthesize different metal species in different proportions (Matteucci, 2003). Therefore, including a model of chemical enrichment in simulations requires specifying the shape of the initial mass function (IMF) for star formation, the lifetimes of stars of different mass and the metal yields from different SN types (see Borgani et al., 2008, for a review). Chemo–dynamical simulations of galaxy clusters have shown that indeed metals are produced at a level comparable with observations (Valdarnini, 2003; Romeo et al., 2006; Tornatore et al., 2007; Kapferer et al., 2007; Davé et al., 2008). Also the resulting spatial distribution of metals is not too different from the observed one, although simulations tend to predict metallicity profiles in the central regions steeper than in observations. This result is generally interpreted as due to the excess of recent star formation taking place in the core regions of simulated clusters (Fabjan et al., 2008).

Since galaxy colors are sensitive to both the star formation rate and the metallicity of the stars, introducing an accurate description of the chemical enrichment opens the possibility to reliably compare the predicted and the observed properties of the cluster galaxy populations. As we have already discussed, hydrodynamical simulations treat the process of star formation through the conversion of cold and dense gas particles into collisionless star particles, treated as single age stellar populations (see § 2). Luminosities in different bands for each particle can be computed using suitable stellar population synthesis models (Bruzual & Charlot, 2003; Silva et al., 1998). Galaxies in simulations can then be identified as gravitationally-bound groups of star particles by a group-finding algorithm (e.g. Klypin et al., 1999; Stadel, 2001; Springel et al., 2001) and their luminosity and colors calculated by summing up luminosities of individual star particles.

These analyses provided results which are quite encouraging as for the level of agreement with observations (Romeo et al., 2005; Saro et al., 2006; Romeo et al., 2008). As an example, we show in Figure 11 the comparison between the observed and simulated V-K vs K color–magnitude relation. The two panels show the results of simulations for two sets of clusters, based on assuming either a standard Salpeter IMF (Salpeter 1955, top panel) or a top–heavy IMF (Arimoto & Yoshii 1987, lower panel) which predicts a much larger number of massive stars and, therefore, of type-II SN. Quite apparently, increasing the number of type-II SN increases the amount of metals produced, with the result that the galaxy population becomes too red. On the other hand, a standard IMF produces fairly realistic galaxies, with a color sequence that reflects a metallicity sequence (i.e. more metal rich galaxies have redder colors). While this is true for the bulk of the galaxy population, simulated BCGs (indicated by the large dots in Figure 11) are much bluer than observed. Again, this is the consequence of the excess of recent star formation in central cluster regions and, as such, represents the evidence in the optical band of the cool-core problem revealed by observations in the X–ray band.

Although there are problems with reproducing luminosities and colors in simulations, the overall spatial distribution of galaxies is reproduced remarkably well (e.g., Nagai & Kravtsov, 2005; Macciò et al., 2006), as is shown in the right plot in Figure 11. The fact that *ab initio* cosmological simulations with simple phenomenological prescriptions for converting gas into stars can match the observed radial distribution of galaxies in clusters is a testament that the hierarchical ΛCDM model of structure formation captures the main processes operating during the formation of clusters.

5   Summary and outlook for the future

In the preceding sections we have discussed the techniques which are currently used to carry out cosmological simulations of cluster formation and reviewed recent progress in the numerical modeling of galaxy clusters. Many of the salient observed properties of clusters, such as scaling relations between observables and total mass, radial profiles of entropy and density of the intracluster gas and radial distribution of galaxies are reproduced quite well. In particular, the outer regions of clusters at radii beyond about 10 per cent of the virial radius are quite regular and exhibit scaling with mass remarkably close to the scaling expected in the simple self-similar model. However, simulations generally do not reproduce the observed "cool core" structure of clusters: simulated clusters generally exhibit a significant amount of cooling in their central regions, which causes both an overestimate of the star formation in the central cluster galaxies and incorrect temperature and entropy profiles. The total baryon fraction in clusters is below the mean universal value and there are interesting tensions between observed stellar and gas fractions in clusters and predictions of simulations. These puzzles point towards an important role played by additional physical processes, beyond those already included in the simulations: plasma transport processes such as viscosity and conduction, AGN powering jets, subsequent injection of turbulence and relativistic particles in bubbles, whose evolution depends on small-scale turbulence, magnetic fields and viscosity.

The observational studies of clusters are increasingly multi-wavelength (IR, optical, X-ray, sub-mm/SZE, radio, gamma-rays). Cosmological simulations of clusters will need to be prepared for the challenge of modeling and interpreting the rich observational datasets which are quickly becoming available. The inclusion of additional physical processes required to reproduce the entire wealth of the data will likely be driving the field of cluster simulations in the near future. Although most of these processes and how they operate in clusters are not well understood, there is a hope that they can be constrained by observations themselves. In this sense, the increasingly sophisticated numerical models of clusters together with multi-wavelength observations serve as an astrophysical laboratory for studying such processes.

As an example, the high-resolution X-ray spectroscopy and (possibly) kinetic SZE will allow us to study the ICM velocity field and constrain the amount and dynamical extension of turbulence. Given that simulations predict that turbulence is ubiquitous in clusters, but its properties are sensitive to viscosity, such observations can constrain viscous energy transport in the intracluster plasma. Large collecting area X-ray telescopes of the next generation along with SZE cluster surveys will allow us to trace evolution of the ICM thermal and chemical properties out to high redshifts ($z > 1 - 1.5$). This will fill the gap between studies of low- to intermediate-z ICM and high-z IGM and trace its evolution with redshift, thereby painting a unified picture of diffuse baryons across a wide range of redshifts.

It may also turn out that too many rather complex processes are shaping the properties of the ICM in cluster cores, and detailed modeling of these regions is fraught with too many uncertainties and problems. Including phenomenological prescriptions for modeling such processes inevitably leads to the loss of the predictive power of the simulations. The practitioners modeling cluster formation (and galaxy formation in general) should figure out how to balance the uncertainties of the included processes with the goal of accurately *predicting* details of observational data. Needless to say, it may not be always possible. This is not a cause for despair as such situations are very common in computational science. In fact, in many problems in physics and astrophysics no exact numerical prediction is possible. Simulations, however, can be very useful even in this case because they can illuminate the ways in which certain processes operate, thereby providing a powerful insight into the physics of the problem and motivating and guiding development of further models (see, e.g., Kadanoff, 2004, for insightful discussion of this issue)

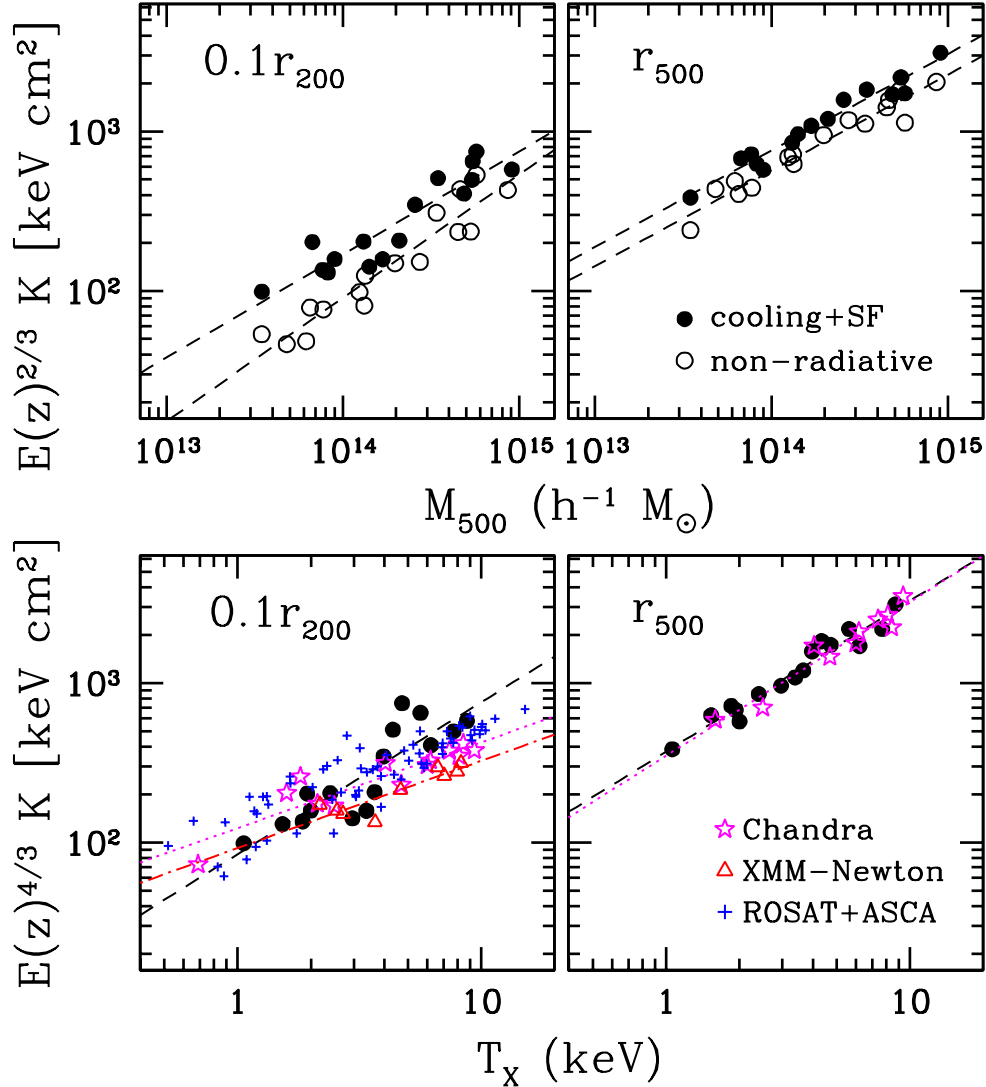[12]Available at $\mathtt{http://jfi.uchicago.edu/} \sim \mathtt{leop/AboutPapers/Computational\_Scenarios.pdf}$

Figure 8: The panels show scaling of ICM entropy ($k_B T/n_e^{2/3}$, where T is the ICM temperature in keV and n_e is its number density of electrons in cm^{-3}) in the cluster core (0.1 of the virial radius, left panels) and at r_{500} (about $0.5r_{200}$, right panels). The upper panels show entropy as a function of total mass within r_{500} for both non-radiative (open circles) simulations and runs with cooling and star formation (solid circles). In the simulations with cooling the lowest entropy gas cools and condenses out of the hot ICM, which results in the higher entropy of the remaining ICM compared to non-radiative simulations. The bottom panels show the entropy in simulations with cooling (solid circles) compared to different observational measurements (as indicated in the legend) as a function of the spectroscopic X-ray temperature of the ICM measured excluding the inner $0.15r_{r500}$ of the cluster from cluster center as a function of the overall X-ray temperature of the ICM. Note that self-similar scaling is $K \propto T_X$. The simulated points are close to the self-similar scaling at both radii. Observations exhibit a weak scaling with temperature in the cluster core $K \propto T_X^{0.5 \pm 0.1}$ indicative of additional physical processes breaking self-similarity of the ICM. At r_{500}, however, both observations and simulations with cooling exhibit scaling close to the self-similar expectation. Based on the results of Nagai et al. (2007a).
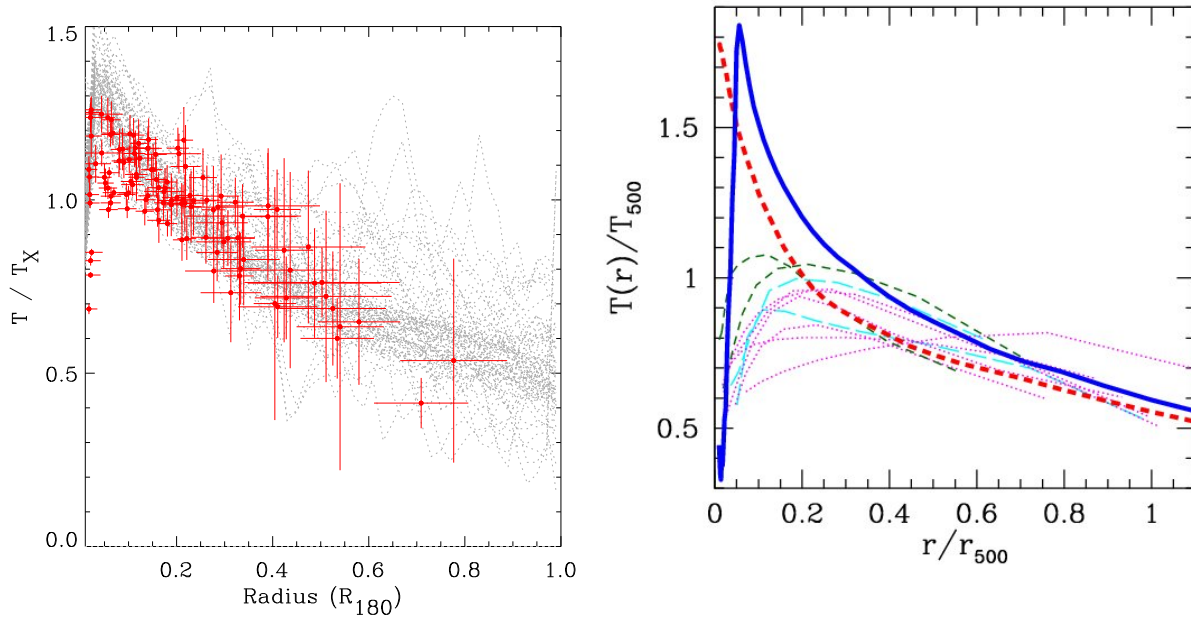
Figure 9: Left panel: comparison between temperature profiles from XMM observations of nearby galaxy clusters (errorbar crosses; Pratt et al. 2007) and simulations (light curves). Figure adopted from Borgani et al. (2004) with copyright permission from 2007 EDP Sciences Ltd. Right panel: comparison between simulated and observed temperature profiles. The heavy solid curve shows the average profiles from an ensemble of clusters simulated including radiative cooling, star formation and a prescription for SN feedback. The heavy dashed curve shows the corresponding result for non–radiative simulations. Lighter curves are the observed temperature profiles for a set of nearby relaxed clusters from Chandra data, analyzed by Vikhlinin et al. (2005). Figure adopted from Nagai et al. (2007a) with copyright permission from 2007 IOP Publishing Ltd.
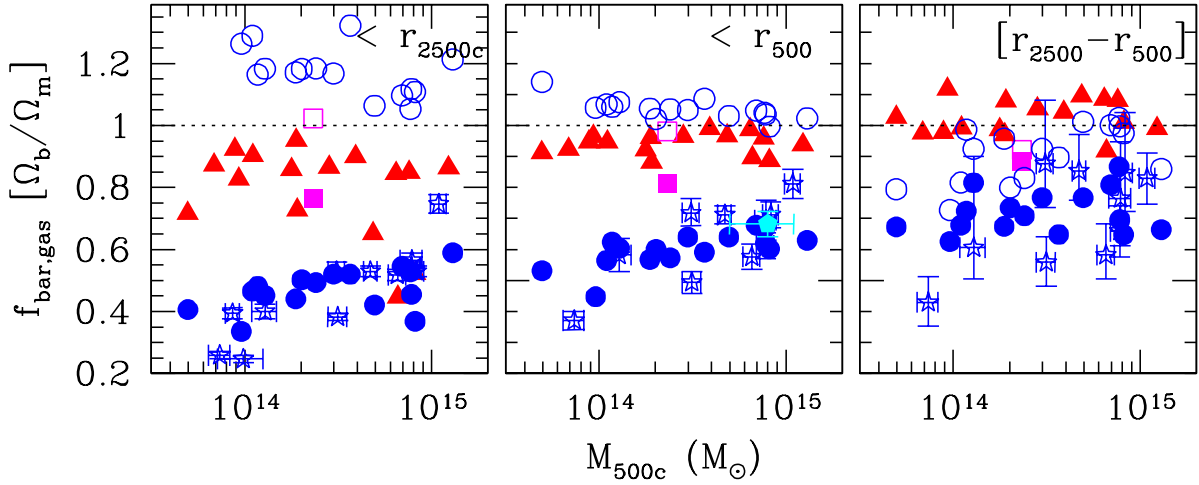
Figure 10: The gas and total baryon fractions of individual clusters in units of the universal mean value within different radii (from the left to the right panels: $r < r_{2500}$, in the annulus $r_{2500}-r_{500}$, $r < r_{500}$) as a function of the cluster mass, M_{500}. *Stars* with error bars show the gas fractions measured for a sample of relaxed clusters using *Chandra* observations (Vikhlinin et al., 2006), while cyan pentagon shows the average value of gas fraction measured in the XMM-DXL sample (Zhang et al., 2008). *Solid triangles* show the gas fractions in the adiabatic simulations. The *solid circles* show the gas fraction, while *open circles* show the total baryon fraction in the simulations with cooling and star formation. *Solid* and *open purple squares* show the gas and baryon fractions in the resimulation of one of the clusters, in which cooling was turned off at $z < 2$. We use the universal baryon fraction of $\Omega_{\mathrm{b}}/\Omega_{\mathrm{m}} = 0.1428$, assumed in cosmological simulations, to normalize the measured cluster gas and baryon fractions, and assume the universal value of $\Omega_{\mathrm{b}}/\Omega_{\mathrm{m}} = 0.17$ for the observed clusters.
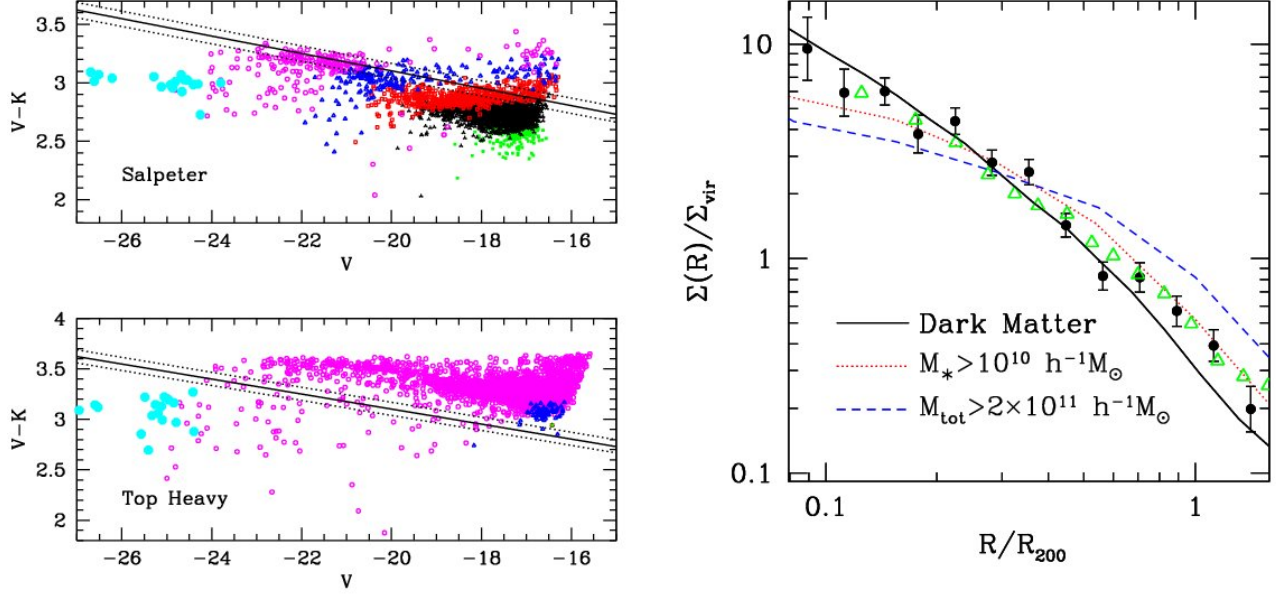
Figure 11: Right panel: the V–K vs. V color–magnitude relation for a set of galaxy clusters simulated with the GADGET-2 code and including a description of chemical enrichment. The top and the bottom panels correspond to assuming a Salpeter (1955) IMF and a top–heavy IMF (Arimoto & Yoshii, 1987), respectively. Straight lines in each panel show the observed CMR relations Bower et al. (1992), with the corresponding intrinsic standard deviations. Big filled dots mark the BCG of each cluster. Different symbols and colors are used for galaxies having different metallicities. Magenta open circles: $Z > 1.5Z_\odot$; blue filled triangles: $1.5 < Z/Z_\odot < 1$; red open squares: $1 < Z/Z_\odot < 0.7$; black open triangles: $0.7 < Z/Z_\odot < 0.4$; green filled squares: $Z < 0.4Z_\odot$. Figure adopted from Saro et al. (2006) with copyright permission from 2006 Blackwell Publishing Ltd. Left panel: projected radial distribution of galactic subhalos $\Sigma(R)/\Sigma_{vir}$ averaged over the eight simulated clusters at $z = 0$ and three orthogonal projections. We show the radial distribution of subhalos selected using the mass thresholds of $M_* > 10^{10}h^{-1}M_\odot$ (*dotted*) and $M_{\rm tot} > 2 \times 10^{11}h^{-1}M_\odot$ (*dashed*). The solid line is the average projected profile of dark matter in the gasdynamics simulation. The *solid circles* are the average radial profile of galaxies in clusters measured in two different surveys (Carlberg et al., 1997; Lin et al., 2004). The data points are scaled arbitrarily. Note that the distribution of M_*-selected subhalos is consistent with the observed distribution of galaxies over the entire range of probed radii: $0.1 < R/R_{200} < 2.0$. Figure adopted from Nagai & Kravtsov (2005) with copyright permission from 2005 IOP Publishing Ltd.

References cited

Aarseth, S. J. 2001, New Astronomy, 6, 277

Abadi, M. G., Bower, R. G., & Navarro, J. F. 2000, MNRAS, 314, 759

Abel, T., Bryan, G. L., & Norman, M. L. 2000, ApJ, 540, 39

Abell, G. O. 1958, ApJS, 3, 211

Agertz, O., Moore, B., Stadel, J., Potter, D., Miniati, F., Read, J., Mayer, L., Gawryszczak, A., Kravtsov, A., Nordlund, Å., Pearce, F., Quilis, V., Rudd, D., Springel, V., Stone, J., Tasker, E., Teyssier, R., Wadsley, J., & Walder, R. 2007, MNRAS, 380, 963

Aharonian, F. & the HESS collaboration. 2008, ArXiv e-prints

Allen, S. W., Rapetti, D. A., Schmidt, R. W., Ebeling, H., Morris, R. G., & Fabian, A. C. 2008, MNRAS, 383, 879

Allen, S. W., Schmidt, R. W., & Fabian, A. C. 2002, MNRAS, 334, L11

Arimoto, N. & Yoshii, Y. 1987, A&A, 173, 23

Arnaud, M. & Evrard, A. E. 1999, MNRAS, 305, 631

Ascasibar, Y., Sevilla, R., Yepes, G., Müller, V., & Gottlöber, S. 2006, MNRAS, 371, 193

Ascasibar, Y., Yepes, G., Müller, V., & Gottlöber, S. 2003, MNRAS, 346, 731

Bagla, J. S. 2002, Journal of Astrophysics and Astronomy, 23, 185

Balbus, S. A. & Reynolds, C. S. 2008, ApJ, 681, L65

Baldi, A., Ettori, S., Mazzotta, P., Tozzi, P., & Borgani, S. 2007, ApJ, 666, 835

Balogh, M. L., Pearce, F. R., Bower, R. G., & Kay, S. T. 2001, MNRAS, 326, 1228

Barnes, J. & Hut, P. 1986, Nature, 324, 446

Baumgartner, W. H., Loewenstein, M., Horner, D. J., & Mushotzky, R. F. 2005, ApJ, 620, 680

Bertschinger, E. 1985, ApJS, 58, 39

Bhattacharya, S., di Matteo, T., & Kosowsky, A. 2008, MNRAS, 389, 34

Bialek, J. J., Evrard, A. E., & Mohr, J. J. 2001, ApJ, 555, 597

Biviano, A. 2000, in Constructing the Universe with Clusters of Galaxies

Bode, P. & Ostriker, J. P. 2003, ApJS, 145, 1

Boehringer, H. & Morfill, G. E. 1988, ApJ, 330, 609

Borgani, S., Fabjan, D., Tornatore, L., Schindler, S., Dolag, K., & Diaferio, A. 2008, Space Science Reviews, 134, 379

Borgani, S., Finoguenov, A., Kay, S. T., Ponman, T. J., Springel, V., Tozzi, P., & Voit, G. M. 2005, MNRAS, 361, 233

Borgani, S., Governato, F., Wadsley, J., Menci, N., Tozzi, P., Lake, G., Quinn, T., & Stadel, J. 2001, ApJ, 559, L71

Borgani, S., Governato, F., Wadsley, J., Menci, N., Tozzi, P., Quinn, T., Stadel, J., & Lake, G. 2002, MNRAS, 336, 409

Borgani, S. & Guzzo, L. 2001, Nature (London) , 409, 39

Borgani, S., Murante, G., Springel, V., Diaferio, A., Dolag, K., Moscardini, L., Tormen, G., Tornatore, L., & Tozzi, P. 2004, MNRAS, 348, 1078

Borgani, S. & Viel, M. 2009, MNRAS, 392, L26

Bouchet, F. R. & Hernquist, L. 1988, ApJS, 68, 521

Bower, R. G., Lucey, J. R., & Ellis, R. S. 1992, MNRAS, 254, 601

Bregman, J. N. & David, L. P. 1988, ApJ, 326, 639

Brighenti, F. & Mathews, W. G. 2003, ApJ, 587, 580

Brüggen, M. & Hoeft, M. 2006, Astronomische Nachrichten, 327, 587

Brüggen, M. & Kaiser, C. R. 2002, Nature (London) , 418, 301

Brunetti, G. & Lazarian, A. 2007, MNRAS, 378, 245

Bruzual, G. & Charlot, S. 2003, MNRAS, 344, 1000

Bryan, G. & Voit, M. 2005, Royal Society of London Philosophical Transactions Series A, 363, 715

Bryan, G. L. 2000, ApJ, 544, L1

Bryan, G. L., Cen, R., Norman, M. L., Ostriker, J. P., & Stone, J. M. 1994, ApJ, 428, 405

Bryan, G. L. & Norman, M. L. 1998, ApJ, 495, 80

Buote, D. A., Gastaldello, F., Humphrey, P. J., Zappacosta, L., Bullock, J. S., Brighenti, F., & Mathews, W. G. 2007, ApJ, 664, 123

Carilli, C. L. & Taylor, G. B. 2002, ARA&A, 40, 319

Carlberg, R. G., Yee, H. K. C., & Ellingson, E. 1997, ApJ, 478, 462

Carlstrom, J. E., Holder, G. P., & Reese, E. D. 2002, ARA&A, 40, 643

Carroll, S. M., Press, W. H., & Turner, E. L. 1992, ARA&A, 30, 499

Cassano, R., Gitti, M., & Brunetti, G. 2008, A&A, 486, L31

Castillo-Morales, A. & Schindler, S. 2003, A&A, 403, 433

Cattaneo, A. & Teyssier, R. 2007, MNRAS, 376, 1547

Cen, R. 1992, ApJS, 78, 341

Cen, R. & Ostriker, J. 1992, ApJ, 393, 22

Chandran, B. D. G. & Cowley, S. C. 1998, Physical Review Letters, 80, 3077

Chieze, J.-P., Alimi, J.-M., & Teyssier, R. 1998, ApJ, 495, 630

Cho, J. & Lazarian, A. 2004, Journal of Korean Astronomical Society, 37, 557

Churazov, E., Brüggen, M., Kaiser, C. R., Böhringer, H., & Forman, W. 2001, ApJ, 554, 261

Churazov, E., Forman, W., Vikhlinin, A., Tremaine, S., Gerhard, O., & Jones, C. 2008, MNRAS, 388, 1062

Conroy, C. & Ostriker, J. P. 2008, ApJ, 681, 151

Couchman, H. M. P. 1991, ApJ, 368, L23

Crain, R. A., Eke, V. R., Frenk, C. S., Jenkins, A., McCarthy, I. G., Navarro, J. F., & Pearce, F. R. 2007, MNRAS, 377, 41

Crocce, M., Pueblas, S., & Scoccimarro, R. 2006, MNRAS, 373, 369

Croston, J. H., Pratt, G. W., Böhringer, H., Arnaud, M., Pointecouteau, E., Ponman, T. J., Sanderson, A. J. R., Temple, R. F., Bower, R. G., & Donahue, M. 2008, A&A, 487, 431

Cuesta, A. J., Prada, F., Klypin, A., & Moles, M. 2008, MNRAS, 389, 385

Dalal, N., Doré, O., Huterer, D., & Shirokov, A. 2008, Phys.Rev.D, 77, 123514

Davé, R., Katz, N., & Weinberg, D. H. 2002, ApJ, 579, 23

Davé, R., Oppenheimer, B. D., & Sivanandam, S. 2008, MNRAS, 391, 110

David, L. P., Jones, C., & Forman, W. 1995, ApJ, 445, 578

De Grandi, S., Ettori, S., Longhetti, M., & Molendi, S. 2004, A&A, 419, 7

Dennis, T. J. & Chandran, B. D. G. 2005, ApJ, 622, 205

Di Matteo, T., Springel, V., & Hernquist, L. 2005, Nature (London) , 433, 604

Diemand, J., Moore, B., Stadel, J., & Kazantzidis, S. 2004, MNRAS, 348, 977

Dolag, K., Bartelmann, M., & Lesch, H. 1999, A&A, 348, 351

—. 2002, A&A, 387, 383

Dolag, K., Borgani, S., Murante, G., & Springel, V. 2008a, ArXiv e-prints

Dolag, K., Bykov, A. M., & Diaferio, A. 2008b, Space Science Reviews, 134, 311

Dolag, K., Evrard, A., & Bartelmann, M. 2001, A&A, 369, 36

Dolag, K., Jubelgas, M., Springel, V., Borgani, S., & Rasia, E. 2004, ApJ, 606, L97

Dolag, K. & Schindler, S. 2000, A&A, 364, 491

Dolag, K. & Stasyszyn, F. A. 2008, ArXiv e-prints

Dolag, K., Vazza, F., Brunetti, G., & Tormen, G. 2005, MNRAS, 364, 753

Donahue, M., Horner, D. J., Cavagnolo, K. W., & Voit, G. M. 2006, ApJ, 643, 730

Dubois, Y. & Teyssier, R. 2008, A&A, 482, L13

Efstathiou, G., Davis, M., White, S. D. M., & Frenk, C. S. 1985, ApJS, 57, 241

Eilek, J., Owen, F., & Marković, T. 2006, Astronomische Nachrichten, 327, 567

Eilek, J. A. & Owen, F. N. 2002, ApJ, 567, 202

Eke, V. R., Cole, S., & Frenk, C. S. 1996, MNRAS, 282, 263

Eke, V. R., Navarro, J. F., & Frenk, C. S. 1998, ApJ, 503, 569

El-Zant, A. A., Kim, W.-T., & Kamionkowski, M. 2004, MNRAS, 354, 169

Ettori, S. 2003, MNRAS, 344, L13

Ettori, S. & Brighenti, F. 2008, MNRAS, 387, 631

Ettori, S., Dolag, K., Borgani, S., & Murante, G. 2006, MNRAS, 365, 1021

Ettori, S. & Fabian, A. C. 1999, MNRAS, 305, 834

Ettori, S., Tozzi, P., & Rosati, P. 2003, A&A, 398, 879

Evrard, A. E. 1988, MNRAS, 235, 911

—. 1990, ApJ, 363, 349

Evrard, A. E. & Henry, J. P. 1991, ApJ, 383, 95

Evrard, A. E., Metzler, C. A., & Navarro, J. F. 1996, ApJ, 469, 494

Evrard, A. E., Summers, F. J., & Davis, M. 1994, ApJ, 422, 11

Fabian, A. C. 1994, ARA&A, 32, 277

Fabjan, D., Tornatore, L., Borgani, S., Saro, A., & Dolag, K. 2008, MNRAS, 386, 1265

Faltenbacher, A., Kravtsov, A. V., Nagai, D., & Gottlöber, S. 2005, MNRAS, 358, 139

Frenk, C. S., Evrard, A. E., White, S. D. M., & Summers, F. J. 1996, ApJ, 472, 460

Frenk, C. S., White, S. D. M., Bode, P., Bond, J. R., Bryan, G. L., Cen, R., Couchman, H. M. P., Evrard, A. E., Gnedin, N., Jenkins, A., Khokhlov, A. M., Klypin, A., Navarro, J. F., Norman, M. L., Ostriker, J. P., Owen, J. M., Pearce, F. R., Pen, U.-L., Steinmetz, M., Thomas, P. A., Villumsen, J. V., Wadsley, J. W., Warren, M. S., Xu, G., & Yepes, G. 1999, ApJ, 525, 554

Gnedin, N. Y. 1995, ApJS, 97, 231

Gonzalez, A. H., Zaritsky, D., & Zabludoff, A. I. 2007, ApJ, 666, 147

Govoni, F. & Feretti, L. 2004, International Journal of Modern Physics D, 13, 1549

Grossi, M., Branchini, E., Dolag, K., Matarrese, S., & Moscardini, L. 2008, MNRAS, 390, 438

Guo, F. & Oh, S. P. 2008, MNRAS, 384, 251

Gursky, H., Kellogg, E., Murray, S., Leong, C., Tananbaum, H., & Giacconi, R. 1971, ApJ, 167, L81+

Hockney, R. & Eastwood, J. 1988, Computer simulations using particles (Bristol and Philadelphia: Institute of Physics Publishing)

Hubble, E. P. 1925, The Observatory, 48, 139

—. 1926, ApJ, 64, 321

Iapichino, L. & Niemeyer, J. C. 2008, MNRAS, 388, 1089

Inogamov, N. A. & Sunyaev, R. A. 2003, Astronomy Letters, 29, 791

Inutsuka, S.-I. 2002, Journal of Computational Physics, 179, 238

Kadanoff, L. 2004, Physics Today, 11

Kaiser, N. 1986, MNRAS, 222, 323

—. 1991, ApJ, 383, 104

Kang, H., Cen, R., Ostriker, J. P., & Ryu, D. 1994, ApJ, 428, 1

Kang, H., Ryu, D., Cen, R., & Ostriker, J. P. 2007, ApJ, 669, 729

Kapferer, W., Kronberger, T., Weratschnig, J., Schindler, S., Domainko, W., van Kampen, E., Kimeswenger, S., Mair, M., & Ruffert, M. 2007, A&A, 466, 813

Katz, N. 1992, ApJ, 391, 502

Katz, N. & Gunn, J. E. 1991, ApJ, 377, 365

Katz, N., Weinberg, D. H., & Hernquist, L. 1996, ApJS, 105, 19

Katz, N. & White, S. D. M. 1993, ApJ, 412, 455

Kay, S., Pearce, F., Frenk, C., & Jenkins, A. 2002, MNRAS, in press, (astro-ph/0106462)

Kay, S. T., Thomas, P. A., Jenkins, A., & Pearce, F. R. 2004, MNRAS, 355, 1091

Kellogg, E., Gursky, H., Leong, C., Schreier, E., Tananbaum, H., & Giacconi, R. 1971, ApJ, 165, L49+

Kim, W.-T. 2007, ApJ, 667, L5

Kim, W.-T., El-Zant, A. A., & Kamionkowski, M. 2005, ApJ, 632, 157

Kim, W.-T. & Narayan, R. 2003, ApJ, 596, 889

Klypin, A., Gottlöber, S., Kravtsov, A. V., & Khokhlov, A. M. 1999, ApJ, 516, 530

Klypin, A. A. & Shandarin, S. F. 1983, MNRAS, 204, 891

Knebe, A., Kravtsov, A. V., Gottlöber, S., & Klypin, A. A. 2000, MNRAS, 317, 630

Komatsu, E., Dunkley, J., Nolta, M. R., Bennett, C. L., Gold, B., Hinshaw, G., Jarosik, N., Larson, D., Limon, M., Page, L., Spergel, D. N., Halpern, M., Hill, R. S., Kogut, A., Meyer, S. S., Tucker, G. S., Weiland, J. L., Wollack, E., & Wright, E. L. 2008, ArXiv e-prints

Kosowsky, A. 2003, New Astronomy Review, 47, 939

Kravtsov, A. V., Klypin, A., & Hoffman, Y. 2002, ApJ, 571, 563

Kravtsov, A. V., Nagai, D., & Vikhlinin, A. A. 2005, ApJ, 625, 588

Kravtsov, A. V. & Yepes, G. 2000, MNRAS, 318, 227

Laney, C. 1998, Computational gasdynamics (Cambridge: CUP)

LaRoque, S. J., Bonamente, M., Carlstrom, J. E., Joy, M. K., Nagai, D., Reese, E. D., & Dawson, K. S. 2006, ApJ, 652, 917

Lau, E., Kravtsov, A., & Nagai, D. 2009, ApJ to be submitted

Leccardi, A. & Molendi, S. 2008, A&A, 487, 461

Lin, W. P., Jing, Y. P., Mao, S., Gao, L., & McCarthy, I. G. 2006, ApJ, 651, 636

Lin, Y.-T., Mohr, J. J., & Stanford, S. A. 2003, ApJ, 591, 749

—. 2004, ApJ, 610, 745

Loeb, A. 2007, Journal of Cosmology and Astro-Particle Physics, 3, 1

Loken, C., Norman, M. L., Nelson, E., Burns, J., Bryan, G. L., & Motl, P. 2002, ApJ, 579, 571

Macciò, A. V., Moore, B., Stadel, J., & Diemand, J. 2006, MNRAS, 366, 1529

Mahdavi, A., Hoekstra, H., Babul, A., & Henry, J. P. 2008, MNRAS, 384, 1567

Malyshkin, L. 2001, ApJ, 554, 561

Markevitch, M. 1998, ApJ, 504, 27

Markevitch, M. & Vikhlinin, A. 2007, Phys. Reports, 443, 1

Mathews, W. G. & Brighenti, F. 2007, ApJ, 660, 1137

Matteucci, F. 2003, The Chemical Evolution of the Galaxy (The Chemical Evolution of the Galaxy. By Francesca Matteucci, Department of Astronomy, University of Trieste, Italy. Astrophysics and Space Science Library Volume 253 reprint Kluwer Academic Publishers, Dordrecht)

Maughan, B. J., Jones, C., Jones, L. R., & Van Speybroeck, L. 2007, ApJ, 659, 1125

Mayer, L., Governato, F., & Kaufmann, T. 2008, ArXiv e-prints

McCarthy, I. G., Bower, R. G., & Balogh, M. L. 2007a, MNRAS, 377, 1457

McCarthy, I. G., Bower, R. G., Balogh, M. L., Voit, G. M., Pearce, F. R., Theuns, T., Babul, A., Lacey, C. G., & Frenk, C. S. 2007b, MNRAS, 376, 497

McNamara, B. R. & Nulsen, P. E. J. 2007, ARA&A, 45, 117

Metzler, C. A. & Evrard, A. E. 1994, ApJ, 437, 564

—. 1997, preprint (astro-ph/9710324)

Miley, G. K., Overzier, R. A., Zirm, A. W., Ford, H. C., Kurk, J., Pentericci, L., Blakeslee, J. P., Franx, M., Illingworth, G. D., Postman, M., Rosati, P., Röttgering, H. J. A., Venemans, B. P., & Helder, E. 2006, ApJ, 650, L29

Miniati, F., Ryu, D., Kang, H., Jones, T. W., Cen, R., & Ostriker, J. P. 2000, ApJ, 542, 608

Mitchell, N. L., McCarthy, I. G., Bower, R. G., Theuns, T., & Crain, R. A. 2008, ArXiv e-prints

Mohr, J. J. & Evrard, A. E. 1997, ApJ, 491, 38

Molendi, S. & Gastaldello, F. 2009, A&A, 493, 13

Monaghan, J. J. 2005, Reports on Progress in Physics, 68, 1703

Morris, J. P. & Monaghan, J. J. 1997, J. Comput. Phys., 136, 41

Muanwong, O., Kay, S. T., & Thomas, P. A. 2006, ApJ, 649, 640

Muanwong, O., Thomas, P. A., Kay, S. T., & Pearce, F. R. 2002, MNRAS, 336, 527

Muanwong, O., Thomas, P. A., Kay, S. T., Pearce, F. R., & Couchman, H. M. P. 2001, ApJ, 552, L27

Murante, G., Giovalli, M., Gerhard, O., Arnaboldi, M., Borgani, S., & Dolag, K. 2007, MNRAS, 377, 2

Nagai, D. & Kravtsov, A. V. 2003, ApJ, 587, 514

—. 2005, ApJ, 618, 557

Nagai, D., Kravtsov, A. V., & Kosowsky, A. 2003, ApJ, 587, 524

Nagai, D., Kravtsov, A. V., & Vikhlinin, A. 2007a, ApJ, 668, 1

Nagai, D., Vikhlinin, A., & Kravtsov, A. V. 2007b, ApJ, 655, 98

Narayan, R. & Medvedev, M. V. 2001, ApJ, 562, L129

Navarro, J. F., Frenk, C. S., & White, S. D. M. 1995a, MNRAS, 275, 720

Navarro, J. F., Frenk, C. S., & White, S. D. M. 1995b, MNRAS, 275, 720

Norman, M. L. & Bryan, G. L. 1999, in Lecture Notes in Physics, Berlin Springer Verlag, Vol. 530, The Radio Galaxy Messier 87, ed. H.-J. Röser & K. Meisenheimer, 106–+

Omma, H. & Binney, J. 2004, MNRAS, 350, L13

Omma, H., Binney, J., Bryan, G., & Slyz, A. 2004, MNRAS, 348, 1105

Osmond, J. P. F. & Ponman, T. J. 2004, MNRAS, 350, 1511

Overzier, R. A., Bouwens, R. J., Cross, N. J. G., Venemans, B. P., Miley, G. K., Zirm, A. W., Benítez, N., Blakeslee, J. P., Coe, D., Demarco, R., Ford, H. C., Homeier, N. L., Illingworth, G. D., Kurk, J. D., Martel, A. R., Mei, S., Oliveira, I., Röttgering, H. J. A., Tsvetanov, Z. I., & Zheng, W. 2008, ApJ, 673, 143

Pearce, F. R., Thomas, P. A., Couchman, H. M. P., & Edge, A. C. 2000, MNRAS, 317, 1029

Peebles, P. J. E. 1970, AJ, 75, 13

—. 1993, Principles of physical cosmology (Princeton Series in Physics, Princeton, NJ: Princeton University Press, —c1993)

Pen, U. 1998, ApJS, 115, 19

Pen, U.-L. 1997, New Astronomy, 2, 309

Perkins, J. S., Badran, H. M., Blaylock, G., Bradbury, S. M., Cogan, P., Chow, Y. C. K., Cui, W., Daniel, M. K., Falcone, A. D., Fegan, S. J., Finley, J. P., Fortin, P., Fortson, L. F., Gillanders, G. H., Gutierrez, K. J., Grube, J., Hall, J., Hanna, D., Holder, J., Horan, D., Hughes, S. B., Humensky, T. B., Kenny, G. E., Kertzman, M., Kieda, D. B., Kildea, J., Kosack, K., Krawczynski, H., Krennrich, F., Lang, M. J., LeBohec, S., Maier, G., Moriarty, P., Ong, R. A., Pohl, M., Ragan, K., Rebillot, P. F., Sembroski, G. H., Steele, D., Swordy, S. P., Valcarcel, L., Vassiliev, V. V., Wakely, S. P., Weekes, T. C., & Williams, D. A. 2006, ApJ, 644, 148

Peterson, J. R. & Fabian, A. C. 2006, Phys.Reports, 427, 1

Pfrommer, C., Springel, V., Enßlin, T. A., & Jubelgas, M. 2006, MNRAS, 367, 113

Piffaretti, R. & Valdarnini, R. 2008, A&A, 491, 71

Pillepich, A., Porciani, C., & Hahn, O. 2008, ArXiv e-prints

Ponman, T. J., Sanderson, A. J. R., & Finoguenov, A. 2003, MNRAS, 343, 331

Power, C., Navarro, J. F., Jenkins, A., Frenk, C. S., White, S. D. M., Springel, V., Stadel, J., & Quinn, T. 2003, MNRAS, 338, 14

Pratt, G. W., Böhringer, H., Croston, J. H., Arnaud, M., Borgani, S., Finoguenov, A., & Temple, R. F. 2007, A&A, 461, 71

Pratt, G. W., Croston, J. H., Arnaud, M., & Boehringer, H. 2008, ArXiv e-prints

Price, D. J. 2008, Journal of Computational Physics, 227, 10040

Prunet, S., Pichon, C., Aubert, D., Pogosyan, D., Teyssier, R., & Gottloeber, S. 2008, ApJS, 178, 179

Puchwein, E., Sijacki, D., & Springel, V. 2008, ApJ, 687, L53

Quilis, V., Bower, R. G., & Balogh, M. L. 2001, MNRAS, 328, 1091

Rafferty, D. A., McNamara, B. R., Nulsen, P. E. J., & Wise, M. W. 2006, ApJ, 652, 216

Rasera, Y. & Chandran, B. 2008, ApJ, 685, 105

Rasia, E., Ettori, S., Moscardini, L., Mazzotta, P., Borgani, S., Dolag, K., Tormen, G., Cheng, L. M., & Diaferio, A. 2006, MNRAS, 369, 2013

Rasia, E., Tormen, G., & Moscardini, L. 2004, MNRAS, 351, 237

Rebusco, P., Churazov, E., Böhringer, H., & Forman, W. 2005, MNRAS, 359, 1041

Renzini, A. 1997, ApJ, 488, 35

Rephaeli, Y. & Silk, J. 1995, ApJ, 442, 91

Reynolds, C. S., McKernan, B., Fabian, A. C., Stone, J. M., & Vernaleo, J. C. 2005, MNRAS, 357, 242

Ricker, P. M. & Sarazin, C. L. 2001, ApJ, 561, 621

Roediger, E. & Brüggen, M. 2008, MNRAS, 388, L89

Roettiger, K., Stone, J. M., & Burns, J. O. 1999, ApJ, 518, 594

Romeo, A. D., Napolitano, N. R., Covone, G., Sommer-Larsen, J., Antonuccio-Delogu, V., & Capaccioli, M. 2008, MNRAS, 389, 13

Romeo, A. D., Portinari, L., & Sommer-Larsen, J. 2005, MNRAS, 361, 983

Romeo, A. D., Sommer-Larsen, J., Portinari, L., & Antonuccio-Delogu, V. 2006, MNRAS, 371, 548

Roncarelli, M., Ettori, S., Dolag, K., Moscardini, L., Borgani, S., & Murante, G. 2006, MNRAS, 373, 1339

Rosati, P., Borgani, S., & Norman, C. 2002, ARA&A, 40, 539

Roussel, H., Sadat, R., & Blanchard, A. 2000, A&A, 361, 429

Ruhl, J., Ade, P. A. R., Carlstrom, J. E., & et al. 2004, in Presented at the Society of Photo-Optical Instrumentation Engineers (SPIE) Conference, Vol. 5498, Society of Photo-Optical Instrumentation Engineers (SPIE) Conference Series, ed. C. M. Bradford, P. A. R. Ade, J. E. Aguirre, J. J. Bock, M. Dragovan, L. Duband, L. Earle, J. Glenn, H. Matsuhara, B. J. Naylor, H. T. Nguyen, M. Yun, & J. Zmuidzinas, 11–29

Ruszkowski, M. & Begelman, M. C. 2002, ApJ, 581, 223

Ruszkowski, M., Brüggen, M., & Begelman, M. C. 2004, ApJ, 611, 158

Ruszkowski, M., Enßlin, T. A., Brüggen, M., Begelman, M. C., & Churazov, E. 2008, MNRAS, 383, 1359

Ryu, D., Kang, H., Hallman, E., & Jones, T. W. 2003, ApJ, 593, 599

Salpeter, E. E. 1955, ApJ, 121, 161

Sanders, J. S. & Fabian, A. C. 2007, MNRAS, 381, 1381

Sarazin, C. L. 1986, Reviews of Modern Physics, 58, 1

Saro, A., Borgani, S., Tornatore, L., De Lucia, G., Dolag, K., & Murante, G. 2009, MNRAS, 392, 795

Saro, A., Borgani, S., Tornatore, L., Dolag, K., Murante, G., Biviano, A., Calura, F., & Charlot, S. 2006, MNRAS, 373, 397

Sasaki, S. 1996, PASJ, 48, L119

Schindler, S. 2002, in Astrophysics and Space Science Library, Vol. 272, Merging Processes in Galaxy Clusters, ed. L. Feretti, I. M. Gioia, & G. Giovannini, 229–251

Schindler, S. & Diaferio, A. 2008, Space Science Reviews, 134, 363

Schuecker, P., Finoguenov, A., Miniati, F., Böhringer, H., & Briel, U. G. 2004, A&A, 426, 387

Seljak, U., Sugiyama, N., White, M., & Zaldarriaga, M. 2003, Phys.Rev.D, 68, 083507

Shang, C., Crotts, A., & Haiman, Z. 2007, ApJ, 671, 136

Sijacki, D., Pfrommer, C., Springel, V., & Enßlin, T. A. 2008, MNRAS, 387, 1403

Sijacki, D. & Springel, V. 2006, MNRAS, 366, 397

Sijacki, D., Springel, V., di Matteo, T., & Hernquist, L. 2007, MNRAS, 380, 877

Silva, L., Granato, G. L., Bressan, A., & Danese, L. 1998, ApJ, 509, 103

Sirko, E. 2005, ApJ, 634, 728

Smith, S. 1936, ApJ, 83, 23

Snowden, S. L., Mushotzky, R. F., Kuntz, K. D., & Davis, D. S. 2008, A&A, 478, 615

Spiegel, E. A. & Thiffeault, J.-L. 2003, Physics of Fluids, 15, 3558

Spitzer, L. 1962, Physics of Fully Ionized Gases (Physics of Fully Ionized Gases, New York: Interscience (2nd edition), 1962)

Springel, V. 2005, MNRAS, 364, 1105

—. 2009, MNRAS submitted (astro-ph/0901.4107)

Springel, V. & Hernquist, L. 2003a, MNRAS, 339, 289

—. 2003b, MNRAS, 339, 312

Springel, V., White, S., Tormen, G., & Kauffmann, G. 2001, MNRAS, 328, 726

Stadel, J. G. 2001, Ph.D. Thesis

Staniszewski, Z., Ade, P. A. R., Aird, K. A., Benson, B. A., Bleem, L. E., Carlstrom, J. E., Chang, C. L., Cho, H. ., Crawford, T. M., Crites, A. T., de Haan, T., Dobbs, M. A., Halverson, N. W., Holder, G. P., Holzapfel, W. L., Hrubes, J. D., Joy, M., Keisler, R., Lanting, T. M., Lee, A. T., Leitch, E. M., Loehr, A., Lueker, M., McMahon, J. J., Mehl, J., Meyer, S. S., Mohr, J. J., Montroy, T. E., Ngeow, C. ., Padin, S., Plagge, T., Pryke, C., Reichardt, C. L., Ruhl, J. E., Schaffer, K. K., Shaw, L., Shirokoff, E., Spieler, H. G., Stalder, B., Stark, A. A., Vanderlinde, K., Vieira, J. D., Zahn, O., & Zenteno, A. 2008, ArXiv e-prints

Subramanian, K., Shukurov, A., & Haugen, N. E. L. 2006, MNRAS, 366, 1437

Sun, M., Voit, G. M., Donahue, M., Jones, C., & Forman, W. 2008, ApJ in press (astro-ph/0805.2320)

Sunyaev, R. A., Norman, M. L., & Bryan, G. L. 2003, Astronomy Letters, 29, 783

Sunyaev, R. A. & Zeldovich, I. B. 1980, ARA&A, 18, 537

Sunyaev, R. A. & Zeldovich, Y. B. 1970, Comments on Astrophysics and Space Physics, 2, 66

—. 1972, Comments on Astrophysics and Space Physics, 4, 173

Sutherland, R. S. & Dopita, M. A. 1993, ApJS, 88, 253

Takizawa, M. 1999, ApJ, 520, 514

Tasker, E. J., Brunino, R., Mitchell, N. L., Michielsen, D., Hopton, S., Pearce, F. R., Bryan, G. L., & Theuns, T. 2008, MNRAS, 390, 1267

Teyssier, R. 2002, A&A, 385, 337

Teyssier, R., Chièze, J.-P., & Alimi, J.-M. 1998, ApJ, 509, 62

Thomas, P. A. & Couchman, H. M. P. 1992, MNRAS, 257, 11

Tornatore, L., Borgani, S., Dolag, K., & Matteucci, F. 2007, MNRAS, 382, 1050

Tornatore, L., Borgani, S., Springel, V., Matteucci, F., Menci, N., & Murante, G. 2003, MNRAS, 342, 1025

Tozzi, P. & Norman, C. 2001, ApJ, 546, 63

Tribble, P. C. 1989, MNRAS, 238, 1247

Tucker, W. H. & Rosner, R. 1983, ApJ, 267, 547

Valdarnini, R. 2002, ApJ, 567, 741

—. 2003, MNRAS, 339, 1117

Vernaleo, J. C. & Reynolds, C. S. 2006, ApJ, 645, 83

Vikhlinin, A., Burenin, R. A., Ebeling, H., Forman, W. R., Hornstrup, A., Jones, C., Kravtsov, A. V., Murray, S. S., Nagai, D., Quintana, H., & Voevodkin, A. 2008, ArXiv e-prints

Vikhlinin, A., Kravtsov, A., Forman, W., Jones, C., Markevitch, M., Murray, S. S., & Van Speybroeck, L. 2006, ApJ, 640, 691

Vikhlinin, A., Markevitch, M., Murray, S. S., Jones, C., Forman, W., & Van Speybroeck, L. 2005, ApJ, 628, 655

Voigt, L. M. & Fabian, A. C. 2004, MNRAS, 347, 1130

Voit, G. M. 2005, Reviews of Modern Physics, 77, 207

Voit, G. M., Balogh, M. L., Bower, R. G., Lacey, C. G., & Bryan, G. L. 2003, ApJ, 593, 272

Voit, G. M. & Bryan, G. L. 2001, Nature (London) , 414, 425

Voit, G. M., Kay, S. T., & Bryan, G. L. 2005, MNRAS, 364, 909

Voit, G. M. & Ponman, T. J. 2003, ApJ, 594, L75

Wadsley, J. W., Veeravalli, G., & Couchman, H. M. P. 2008, MNRAS, 387, 427

Werner, N., Durret, F., Ohashi, T., Schindler, S., & Wiersma, R. P. C. 2008, Space Science
        Reviews, 134, 337

Werner, N., Kaastra, J. S., Takei, Y., Lieu, R., Vink, J., & Tamura, T. 2007, A&A, 468, 849

White, D. A. & Fabian, A. C. 1995, MNRAS, 273, 72

White, S. D. M. 1976, MNRAS, 177, 717

White, S. D. M., Navarro, J. F., Evrard, A. E., & Frenk, C. S. 1993, Nature (London) , 366,
        429+

Wu, X.-P. & Xue, Y.-J. 2002, ApJ, 572, L19

Yepes, G., Kates, R., Khokhlov, A., & Klypin, A. 1997, MNRAS, 284, 235

Yoshida, N., Furlanetto, S. R., & Hernquist, L. 2005, ApJ, 618, L91

Yoshikawa, K., Jing, Y. P., & Suto, Y. 2000, ApJ, 535, 593

Younger, J. D. & Bryan, G. L. 2007, ApJ, 666, 647

Zel'dovich, Ya. B. 1970, 6, 164

Zhang, Y.-Y., Böhringer, H., Finoguenov, A., Ikebe, Y., Matsushita, K., Schuecker, P., Guzzo,
        L., & Collins, C. A. 2006, A&A, 456, 55

Zhang, Y.-Y., Finoguenov, A., Böhringer, H., Kneib, J.-P., Smith, G. P., Kneissl, R., Okabe, N.,
        & Dahle, H. 2008, A&A, 482, 451

Zwicky, F. 1933, Helvetica Physica Acta, 6, 110

—. 1937, ApJ, 86, 217

Zwicky, F., Herzog, E., & Wild, P. 1961, Catalogue of galaxies and of clusters of galaxies, Vol. I
        (Pasadena: California Institute of Technology (CIT), —c1961)